Spectroscopic Studies of Ball Plasmoid Discharges at Atmospheric Pressure

Scott E. Dubowsky

Prospectus for Preliminary Examination

28th March, 2016 2:00 PM

171 Roger Adams Laboratory

University of Illinois at Urbana-Champaign

1 Introduction

Ball plasmoids are the result of a unique type of plasma discharge performed in air. A "plasmoid" is defined as a plasma-magnetic entity [1]; in other words a plasmoid is a plasma which has some definite shape but is not confined to a power source. Early work on plasmoids described toroidal-type systems, however spherical (ball) plasmoids have been shown to be formed with the proper electrode geometry. Typical recombination rates of ambient plasmas with similar chemistry indicate that the plasmoid should dissipate in less than a millisecond [2, 3], however ball plasmoid discharges have been observed to last several hundred milliseconds. There has been no explanation provided in the literature that fully accounts for this discrepancy, and I am making efforts to elucidate the chemical and physical processes by which ball plasmoids are stabilized.

Water-based ball plasmoid discharges generated by a high-voltage (DC), capacitive discharge over a grounded electrolyte solution were first described by Egorov and Stepanov [4] and were later validated by several other groups [5, 6, 7, 8], including ours [9, 10]. Versteegh et al. [5] have provided the most detailed spectroscopic data pertaining to ball plasmoids to date. They used a "medium" resolution échelle spectrometer and a high-resolution double-pass spectrometer to collect emitted light from the plasmoid in the ultraviolet/visible (300-800 nm) at moderate speeds (no faster than 1 ms; their work is unclear regarding the actual speed of detection). From these measurements, the electron density of the plasmoid was estimated to be 10^{16} cm^{-3} at 10 ms and 10^{14} cm^{-3} at 75 ms using Stark broadening of several atomic lines. The electron temperature was also inferred using atomic line intensity ratio measurements, and was found to decrease from about 5000 K to 2000 K in the first 75 ms of the discharge. Additionally, they observed some molecular emission from OH and CaOH, the former having a rotational temperature of 15,000 K (modeled using LIFBASE [11]) and the latter (a result of the calcium ions present in their electrolyte) comprising most of the red/orange emission from the plasmoid.

Friday et al. [8] have performed measurements pertaining to physical properties of the discharge and the optimization of the discharge electronics. They altered voltage, capacitance, electrolyte conductivity, and electrolyte pH to observe how each parameter specifically affected the lifetime of the plasmoid. This work suggests that there is some optimal voltage

for a given capacitance / electrolyte conductivity which will maximize the lifetime of the plasmoid, but more study is needed. A commercial infrared spectrometer was also used to collect absorption measurements of ball plasmoids for the first time. Signals were observed and attributed to water and water clusters, and some signals indicative of the presence of CO_2 as a product of electrode oxidation were also noted. Finally, schleiren videography showed that the plasmoid consists of a hot inner "core" which is surrounded by a distinct, cool, boundary layer. The index of refraction was also shown to be essentially homogeneous across the plasmoid, which has a density approximately 66% of ambient air.

1.1 Plasmoid discharge mechanics

In my laboratory, ball plasmoids are generated via a high-voltage, high-current, capacitive discharge over a grounded electrolyte; a diagram of the circuitry has been included for reference (Figure 1). During an experimental trial, large parallel-plate capacitors (1.958 mF maximum capacitance) are charged to high voltages (up to 10kV DC), and this energy is delivered to a custom electrode setup contained in a bucket of weakly conductive water (normally a few hundred μSiemen). The cathode is a cylindrical rod which is positioned such that the tip of the electrode protrudes 1-2 mm above the surface of the electrolyte. We use a variety of cathode materials including copper, aluminum, stainless steel, carbon (graphite), and tungsten, each with a six mm diameter. The cathode is insulated from the surrounding aqueous environment with a piece of alumina or quartz tubing with an inner diameter of 6 mm and an outer diameter of 8 mm. This is done in order to electrically isolate the cathode from the electrolyte, in other words to ensure that current will travel above the surface of the electrolyte, rather than through it. The anode is an annular copper ring which surrounds the cathode, but is totally submerged in the electrolyte (several cm below the surface).

An Arduino®Uno microcontroller board controls the timing of several high-voltage relays (see Figure 1), and the same microcontroller is used to record voltage and current measurements via a voltage divider and Hall effect sensor, respectively. Discharge parameters are chosen based both on the geometry of the setup and an optimization of safety to personnel and equipment, therefore no discharges above 7 kV are ever performed due to physical limitations of the equipment (temperature rating of power resistors, arcing concerns, etc.). Future

additions and improvement to the circuitry could allow for larger voltages and capacitances to be used safely and successfully.

Ball plasmoid discharges occur in three sequential stages (Figure 2), the beginnings and ends of which are determined by the current profile of the discharge; these are the pre-initiation, buildup, and detachment phases [12]. The pre-initiation phase begins when the switch that triggers the pulse of current to the electrodes closes. Current begins to flow in small amounts and ionization of water vapor and air near the tip of the cathode begins. When the current density is sufficient to generate a plasma at the tip of the cathode (cathode spot threshold), the buildup phase begins. As the plasma begins to grow at the cathode, contact can be established between the plasma and the large surface area of the air-electrolyte interface. Spider-like streamers then extend across the surface of the electrolyte, allowing current to flow freely. During this stage the plasma grows rapidly and eventually the current reaches a maximum as the plasma rises upward and away from the cathode due to buoyant forces. The point at which the current reaches a maximum (up to 126 Amps have been observed with our discharge system [8]) marks the beginning of the detachment phase. In this stage a luminous plasmoid can be seen for an extended period of time, completely separated from the cathode, before dissipating. I am confident that this phase of ball plasmoid discharges will be the most useful in determining the mechanisms by which ball plasmoids are stabilized.

Typical ball plasmoid discharges last approximately 400 ms and have a diameter of approximately twenty cm at their full size, but slight variations in rise velocity, luminosity, current profile, and lifetime can occur between consecutive discharges (much like natural lightning, no two plasmoids are exactly the same). This issue is being addressed in several ways as this project moves forward in an effort to reduce shot-to-shot variability.

1.2 Ball lightning and ball plasmoids

Many of the observables pertaining to ball plasmoid discharges are also reported to be associated with the mysterious natural phenomenon known as ball lightning, an event that was observed with scientific instrumentation for the first time just two years ago [13]. Over the past several centuries, dozens of eyewitness reports describing luminous fireballs dancing

through the sky (for tens of seconds) have been collected [13, 14], however no satisfactory explanation has been provided for the strange behavior of ball lightning. The first reports of ball-lightning like discharges in the laboratory date back to Tesla's work in Colorado Springs, and over the past century several groups have attempted to replicate what Tesla first described in 1899 [15], with varying degrees of success. Although no one claims that ball plasmoids are exact replications of ball lightning, this laboratory analogue provides the first suitable model for the natural phenomenon from which conclusions about the behavior of ball lightning can be drawn.

2 Completed work

2.1 High-performance ambient mass spectrometry

In order to better understand the behavior and composition of ball plasmoids, it was imperative to analyze the charge carriers present within the plasmoid. Mass spectrometry (MS) is arguably the best analytical method with which to identify the ionic composition of a gas-phase sample, therefore an effort was made to perform mass spectrometric analysis of the discharge. In collaboration with the (former) Perry group, a commercial mass spectrometer was slightly modified to sample the plasmoid, and two different mass analyzers were used to probe the plasmoid's composition.

In short, a stainless steel capillary (held at $\pm$ 35 V DC) was added to the sampling interface of the mass spectrometer; the geometry of the setup allowed the capillary to sample from within the interior of the plasmoid. Two cathode materials were used in this set of experiments, namely copper and tungsten. Copper was chosen for two reasons: the distribution of the naturally occurring isotopes of copper (^{63}Cu and ^{65}Cu) is well known and easily observed via MS, and copper ionizes easily, allowing for the formation of cluster ions around a metallic center. Tungsten was chosen because it is robust and can stand up to repeated trials with minimal degradation. Furthermore, we wanted to minimize any interactions between ions generated during the discharge and electrode materials, especially for studies of low-mass ions; no tungsten ions were observed in the spectra of discharges from a tungsten electrode.

Overview (m/z 30-300) spectra were collected using the Orbitrap mass analyzer, and many cluster ions were observed in these spectra. A linear ion trap mass analyzer was used to measure low-mass (m/z 15-85) ions; we observed the protonated water dimer ($[(H_2O)_2H]^+$) and trimer ($[(H_2O)_3H]^+$) and their deuterated isotopologues over deionized water and D_2O (in separate experiments), and we analyzed the distribution of deuterium in these clusters assuming a two-parameter binomial distribution to show that plasmoid composition is influenced (albeit slightly) by the electrolyte composition. We published a paper detailing plasmoid composition analysis using mass spectrometry [9]; this paper is included below for reference.

2.2 Fourier-transform infrared emission spectroscopy

I have also performed emission spectroscopy of ball plasmoid discharges in the mid-infrared [10]. The motivation for this work was two-fold; to extend the work of Versteegh et al. [5] into the infrared and to validate the molecular assignments made by Friday et al. [8]. Using a commercial FTIR spectrometer (Bruker VERTEX 70) in conjunction with some external optics to focus the emitted light from the plasmoid into the instrument, I recorded spectra from several discharges. Specific details of the experimental setup and procedure are included in the attached article. These spectra showed emission from water and hydroxyl radical, and these data were processed in an attempt to extract rotational temperatures of these molecules. First, however, it was necessary to account for absorption by water and CO_2 along the optical path between the discharge and the instrument. A simulation of CO_2 and water absorption (298 K, 2.06 m pathlength, Lorentzian lineshape; 4 cm^{-1} linewidth, 1 atm) was generated using HITRAN online (http://hitran.iao.ru/) and was applied to the observed data to generate corrected spectra. In each spectrum this resulted in a significant increase in emission signal in the regions where atmospheric CO_2 and water readily self-absorb, however there is little effect on the intensity between 2400-3200 cm^{-1} (where emission from OH is present).

The PGOPHER [16] program was used to fit these (corrected) spectra to simulated spectra of water and hydroxyl radical. At the outset of my rotational analysis I attempted to fit a mixture of both of these molecules to the experimental data, however PGOPHER's

functionality allows for only a single rotational temperature to be floated during fitting. The temperatures of different plasmoid constituent molecules were expected to be rather different from one another, therefore each molecule was fit separately. Furthermore, due to the nonequilibrium nature of the discharge, the different vibrational modes of the same molecule (namely water in the context of this analysis) are expected to have slightly different values for rotational temperature, therefore the bending mode was fit independently of the two stretching modes. The temperatures of the bending and stretching modes of H_2O were determined to be 1900±300 K and 2400±400 K (respectively) and the rotational temperature of OH was found to be 9200±1500 K; numerical results of each of the fits to the bending mode and stretching modes of water and to hydroxyl radical (and some graphical representations of these fits) are included in the attached article.

3 Proposed work

Traditionally, diagnostics of ambient plasmas are carried out via optical emission spectroscopy [17, 18, 19, 20], which is effective but can present several potential obstacles to meaningful data analysis. For example, optical thickness results in the collection of emitted light only from the outermost border of a spherical emitter. This is not an ideal case for plasmoid discharges, as ball plasmoids have been shown to be surrounded by an "envelope" which is cooler than the interior of the plasmoid [5]. It is very likely that the chemistry occurring within the hot center of the plasmoid is different than the chemistry occurring at the plasmoid-air interface.

Due to the limitations of emission spectroscopy and the near impossibility to obtain quantitative concentration information from emission spectra, we propose performing absorption spectroscopy using a broadband dye laser (BDL). Glumac [21] has recently shown that absorption spectroscopy can be performed on optically thick fireballs using a BDL. In this work, a frequency-tripled commercial laser (Nd:YAG, 355 nm, 7 ns pulse, 10 Hz) was used as the pump for commercially available dyes, and a custom-built spectrometer was used to record absorbance measurements. Despite beam attenuations of 98% after passing through the fireball, appreciable signal was measured at the detector and time-resolved absorbance measurements of Al and AlO were performed. Soo et al. [22] have also shown that perform-

ing second harmonic generation (SHG) on the beam from the dye laser (using a nonlinear crystal) can extend the range of this technique into the UV, thereby permitting access to additional atomic and molecular species that could be present in the system in question.

3.1 Characterizing the optical depth

An understanding of the optical depth profile(s) of ball plasmoid discharges is paramount to extracting meaningful data from spectroscopic experiments. In addition to causing emitted light from only the outer edge of the plasmoid to be collected, the optical thickness of the plasmoid dictates the relations that should be used when analyzing spectral intensity [19].

We will determine the optical thickness of the discharge via absorption spectroscopy with a modeless BDL using a setup similar to what is described above [21, 22] (Figure 3 shows a simplified setup of the system that will be used). The dye laser will be passed through the discharge and the attenuation of the beam will be used to quantify the optical depth profile of the discharge as a function of space. The ratio of the incident light intensity to the transmitted light intensity allows for the determination of optical depth via the Beer-Lambert Law. In the proposed experiments, a reference beam is split from the incident beam and is passed outside of the discharge region. This beam is then imaged onto the spectrometer entrance slit below the signal beam such that both the signal and reference spectra are recorded in different regions on the same CCD chip.

There are many advantages to this technique: the irradiance of the beam is quite large and the beam is expected to pass through the plasmoid with only some attenuation (less than that of aluminized fireballs), commercial dyes are available for virtually any wavelength in the visible, and fiber coupled optics reduce the complexity of the optical system. Furthermore, sub-millisecond time resolution will be achieved using precise control of the discharge electronics and the laser in addition to registering and normalization of the current profiles across multiple discharges with a fast data acquisition system. Additionally, beam attenuation measurements can be made at different points in space simultaneously during a discharge using multiple optical techniques (fiber splitters, mirrors, etc.). This approach will allow for a comprehensive description of the optical depth in two dimensions, and as a function of time, to be made.

3.2 Probe spectroscopy

Emission spectroscopy can be particularly useful, however, if something can be said about spatial information. To circumvent the issues of data collection in emission spectroscopy (i.e. collecting emitted light from the surface of the plasmoid rather than the interior), one can take spectra from *inside* the discharge. By using fiber probes which are recessed within stainless steel or ceramic capillaries, it is possible to obtain several spectra from within a discharge simultaneously, with microsecond time resolution.

Therefore, I will perform novel *in situ* measurements of ball plasmoid discharges using this fiber probe technique, using both emission and absorption spectroscopies. To summarize this technique, the probes will be mounted such that the emitted light generated over the lifetime of the plasmoid is collected by each probe. The opposite ends of the fibers are re-arranged into a slit and are used at the inlet of the spectrometer, and the instrument produces spectra from each fiber at the frame rate of the detector. For ball plasmoid studies, the probes will be oriented along the vertical axis of the discharge in order to monitor different regions of interest in a single shot.

There are several advantages to this approach, the main advantage being that local temperatures and chemistry can be measured simultaneously and related to the overall behavior of the plasmoid. Depending on the spacing of the optical fibers, hotter and cooler areas of the plasmoid can be identified and monitored over time; this technique could be used to infer the dynamics of the plasmoid in different areas and phases of the discharge, measurements of which have not yet been reported for this system.

3.3 Molecular targets

3.3.1 Hydroxyl radical

Hydroxyl radical has been shown to be a principal component of ball plasmoid chemistry and is thus an attractive target for analysis [5]. The $A^2\Sigma^+ \rightarrow X^2\Pi$ ($\lambda_{(0,0)}$=306.4 nm [23]) transition of OH has been extensively studied and is a common metric by which plasma parameters are determined, thus the different vibronic bands of this transition will be studied in the context of ball plasmoid discharges. Given the high rotational temperatures of OH that have been

previously reported within the plasmoid [5, 9] we expect a large density of spectral lines to be available in this region (Figure 4).

Although this transition is located in the ultraviolet, the technique described above can still be used to perform absorption measurements. Soo and Glumac [22] have shown that the addition of the appropriate nonlinear crystal (at the proper angle) can generate a coherent UV source from the dye laser beam, thus a similar technique will be applied in this experiment. The resolving power ($\lambda/\Delta\lambda$) of the spectrometer described above has been reported to be 53,000 (0.0075 nm) at 395 nm [21], which will facilitate a thorough Boltzmann analysis of a set of OH transitions in multiple vibronic bands of the A-X transition. This analysis will allow for path-averaged rotational temperatures and number densities of OH to be reported and compared to other temperatures that have been reported for this system. Versteegh et al. [5] have presented a pseudo-rotational analysis of OH generated in ball plasmoid discharges in the UV-visible (using emission spectroscopy), however they were unable to record spectra with adequate time resolution. With the methods described above, we expect to collect spectra much faster than previous experiments performed on this discharge. We also plan on reporting quantitative concentration information of ball plasmoid constituents for the first time.

3.3.2 Nitrogen species

As the principal constituent of ambient air, one would assume that nitrogen plays a critical role in both the formation of laboratory plasmoids as well as the formation of ball lightning. However, as of this writing, no measurements pertaining to nitrogen within ball plasmoids have been undertaken (to our knowledge). An ion that is commonly used in plasma diagnostics is the nitrogen molecular cation (N_2^+), a major component of aurorae and other ambient plasmas. The first negative system ($B^2\Sigma_u^+ \rightarrow X^2\Sigma_g^+$; $\lambda_{(0,0)}$=391.4 nm) of N_2^+ is located in the UV-visible and the Meinel band ($A^2\Pi_u \rightarrow X^2\Sigma_g^+$; $\lambda_{(1,0)}$=918.3 nm) of this ion is located in the near-infrared [24]. Furthermore, the first positive ($B^3\Pi_g \rightarrow A^3\Sigma_u^+$; $\lambda_{(0,0)}$=1051.0 nm) and second positive ($C^3\Pi_u \rightarrow B^3\Pi_g$; $\lambda_{(0,0)}$=337.0 nm) bands of excited nitrogen (N_2*) also fall within the same spectral regions [24] and therefore serve as other attractive targets. As is the case with hydroxyl radical, we expect a large density of spectral

lines at plasmoid temperatures (See Figures 5 and 6). Particular attention will be paid to the lifetime of nitrogen molecules across the discharge; this could relate to the long period of visible emission that can be observed from plasmoid discharges.

4 Conclusion

I have demonstrated several measurements and have elucidated information pertaining to ball plasmoid discharges using a variety of different analytical techniques, including mass spectrometry and emission spectroscopy. Thus far, I have conclusively identified ions present within plasmoid discharges and have shown that the composition of these discharges is not entirely random– the data suggest that plasmoid composition is dictated by electrolyte composition. I have also performed the first emission spectroscopy of these plasmoids in the infrared and am the first to report rotational temperatures of water molecules within ball plasmoids. The rotational temperatures that were extracted from the fits of the observed spectra begin to show the energy distribution among molecules in the plasmoid and confirm the measurements of Versteegh et al. [5], reinforcing the fact that ball plasmoid discharges are highly nonthermal and result in rapid heating and rapid cooling of constituent molecules.

Our future experimental plans are relatively simple in their design, but will provide a plethora of new and valuable data. We will first make improvements to the discharge electronics and data acquisition system to minimize shot-to-shot variability and maximize data collection efficiency, respectively. We will then perform several spectroscopic experiments to measure the optical depth profile of the plasmoid, measure spatially-resolved emission as a function of time, and measure spatially and time-resolved absorption of plasmoid constituents. Additionally, the spatial distribution of these targets will also be probed using the methods described above. I am confident that the implementation of these spectroscopic methods and the molecular targets described above will provide fundamental insight into the nature of ball plasmoid discharges, and by extension other nonequilibrium air plasmas.

References

[1] W. H. Bostick, "Experimental study of ionized matter projected across a magnetic field," *Phys. Rev.*, vol. 104, pp. 292–299, Oct 1956.

[2] P. Xuexia, D. Zechao, J. Pengying, L. Weihua, and L. Xia, "Influence of ionization degrees on the evolutions of charged particles in atmospheric plasma at low altitude," *Plasma Science and Technology*, vol. 14, no. 8, p. 716, 2012.

[3] Y. Sakiyama, D. B. Graves, H.-W. Chang, T. Shimizu, and G. E. Morfill, "Plasma chemistry model of surface microdischarge in humid air and dynamics of reactive neutral species," *Journal of Physics D: Applied Physics*, vol. 45, no. 42, p. 425201, 2012.

[4] A. Egorov and S. Stepanov, "Long-lived plasmoids produced in humid air as analogues of ball lightning," *Technical Physics*, vol. 47, no. 12, pp. 1584–1586, 2002.

[5] A. Versteegh, K. Behringer, U. Fantz, G. Fussmann, B. Jüttner, and S. Noack, "Long-living plasmoids from an atmospheric water discharge," *Plasma Sources Science and Technology*, vol. 17, no. 2, p. 024014, 2008.

[6] N. Hayashi, H. Satomi, T. Kajiwara, and T. Tanabe, "Properties of ball lightning generated by a pulsed discharge on surface of an electrolyte in the atmosphere," *IEEJ Transactions on Electrical and Electronic Engineering*, vol. 3, no. 6, pp. 731–733, 2008.

[7] Y. Sakawa, K. Sugiyama, T. Tanabe, and R. More, "Fireball generation in a water discharge," *Plasma and Fusion Research*, vol. 1, pp. 039–039, 2006.

[8] D. M. Friday, P. B. Broughton, T. A. Lee, G. A. Schutz, J. N. Betz, and C. M. Lindsay, "Further insight into the nature of ball-lightning-like atmospheric pressure plasmoids," *The Journal of Physical Chemistry A*, vol. 117, no. 39, pp. 9931–9940, 2013.

[9] S. E. Dubowsky, D. M. Friday, K. C. Peters, Z. Zhao, R. H. Perry, and B. J. McCall, "Mass spectrometry of atmospheric-pressure ball plasmoids," *International Journal of Mass Spectrometry*, vol. 376, no. 0, pp. 39 – 45, 2015.

[10] S. E. Dubowsky, B. Deutsch, R. Bhargava, and B. J. McCall, "Infrared emission spectroscopy of atmospheric-pressure ball plasmoids," *Journal of Molecular Spectroscopy*, vol. 322, pp. 1 – 8, 2016.

[11] J. Luque and D. R. Crosley, "Lifbase: Database and spectral simulation," Technical Report 99-009, SRI International, 1999.

[12] K. D. Stephan, S. Dumas, L. Komala-Noor, and J. McMinn, "Initiation, growth and plasma characteristics of gatchina water plasmoids," *Plasma Sources Science and Technology*, vol. 22, no. 2, p. 025018, 2013.

[13] J. Cen, P. Yuan, and S. Xue, "Observation of the optical and spectral characteristics of ball lightning," *Phys. Rev. Lett.*, vol. 112, p. 035001, Jan 2014.

[14] W. Charman, "Ball lightning," *Physics Reports*, vol. 54, no. 4, pp. 261 – 306, 1979.

[15] N. Tesla, *Colorado Springs Notes: 1899-1900*. Beograd, Yugoslavia: Nolit, 1978.

[16] C. M. Western, "PGOPHER, A program for simulating rotational, vibrational and electronic structure."

[17] A. Fridman and L. A. Kennedy, *Plasma Physics and Engineering*. Boca Raton: CRC Press, 2 ed., 2011.

[18] M. A. Lieberman and A. J. Lichtenberg, *Principles of Plasma Discharges and Materials Processing*. Hoboken: Wiley, 2 ed., 2005.

[19] H. R. Griem, *Principles of Plasma Spectroscopy*. Cambridge University Press, 1997.

[20] C. O. Laux, T. G. Spence, C. H. Kruger, and R. N. Zare, "Optical diagnostics of atmospheric pressure air plasmas," *Plasma Sources Science and Technology*, vol. 12, no. 2, p. 125, 2003.

[21] N. Glumac, "Absorption spectroscopy measurements in optically dense explosive fireballs using a modeless broadband dye laser," *Appl. Spectrosc.*, vol. 63, pp. 1075–1080, Sep 2009.

[22] M. Soo and N. Glumac, "Ultraviolet absorption spectroscopy in optically dense fireballs using broadband second-harmonic generation of a pulsed modeless dye laser," *Appl. Spectrosc.*, vol. 68, pp. 517–524, May 2014.

[23] K. P. Huber and G. Herzberg, *Molecular Spectra and Molecular Structure, IV: Constants of Diatomic Molecules*. Springer: New York, 1979.

[24] A. Lofthus and P. H. Krupenie, "The spectrum of molecular nitrogen," *Journal of Physical and Chemical Reference Data*, vol. 6, no. 1, pp. 113–307, 1977.

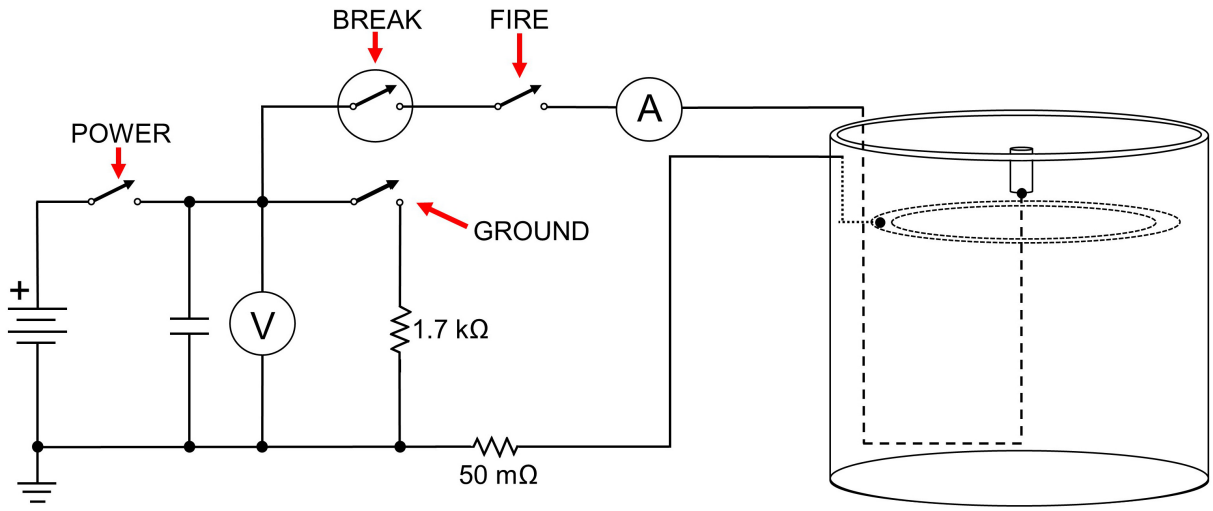

Figure 1: A simplified circuit diagram of the plasmoid discharge circuit. The "POWER" relay delivers current to the capacitor bank, the "FIRE" relay delivers the pulse to the electrodes, "BREAK" is the vacuum relay which breaks current to the electrodes, and finally the "GROUND" relay grounds the system. V and A are a voltage divider and a Hall effect current sensor, respectively.

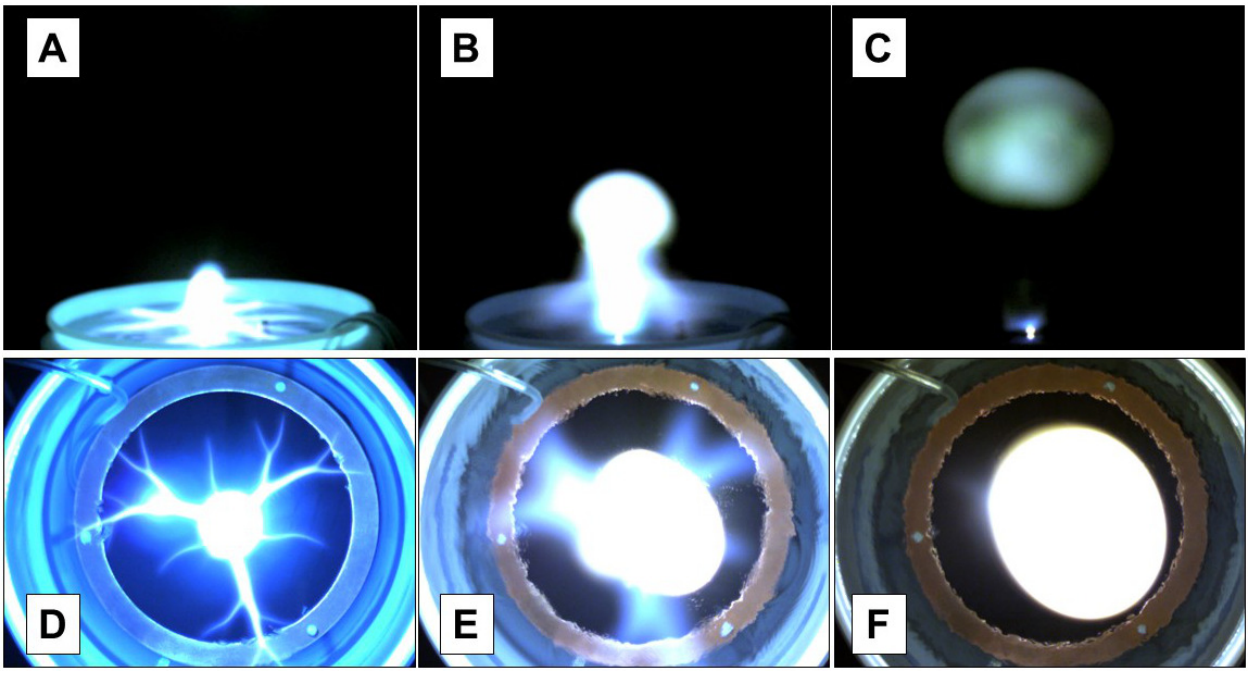

Figure 2: Images obtained from high-speed videography of plasmoid discharges. A-C: initiation, propagation, and detachment phases of the discharge. D-F: top-down view of the same phases shown in A-C, taken from a discharge with the same parameters on the same day. High-speed videography is performed with a Pixelink®PL-B&42U camera with a frame rate of 98 fps.

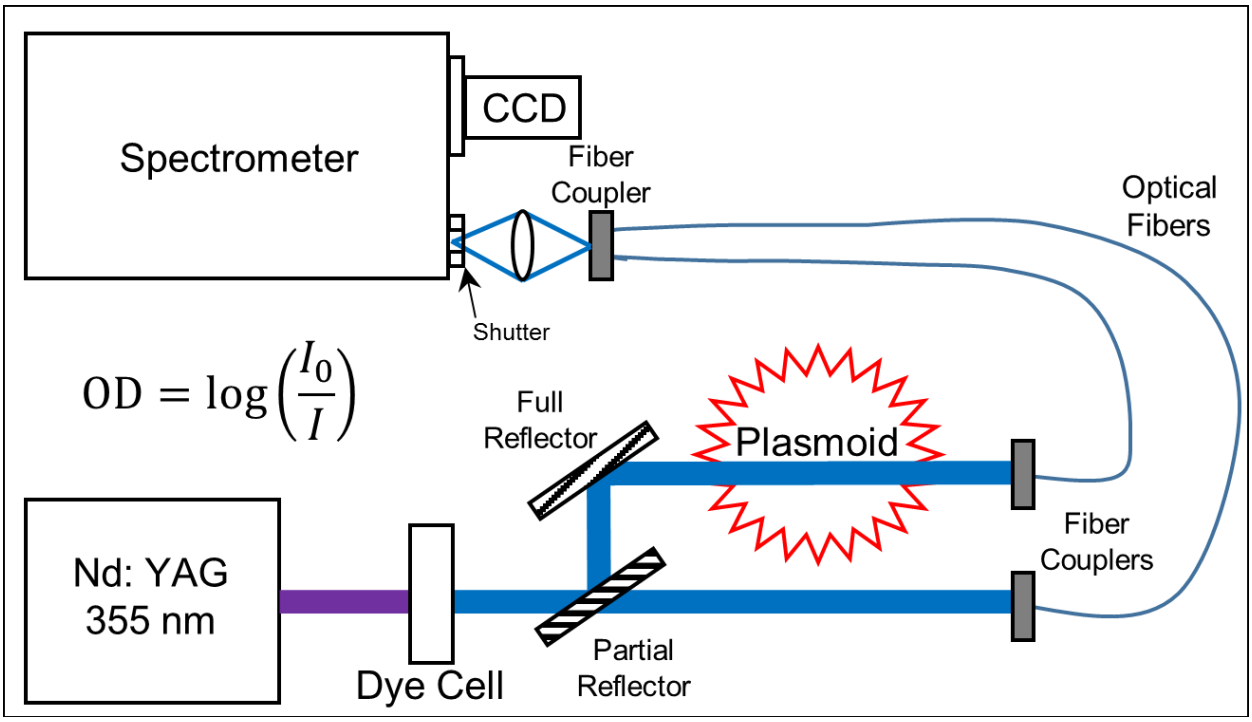

Figure 3: Simplified diagram of the proposed spectroscopic setup.

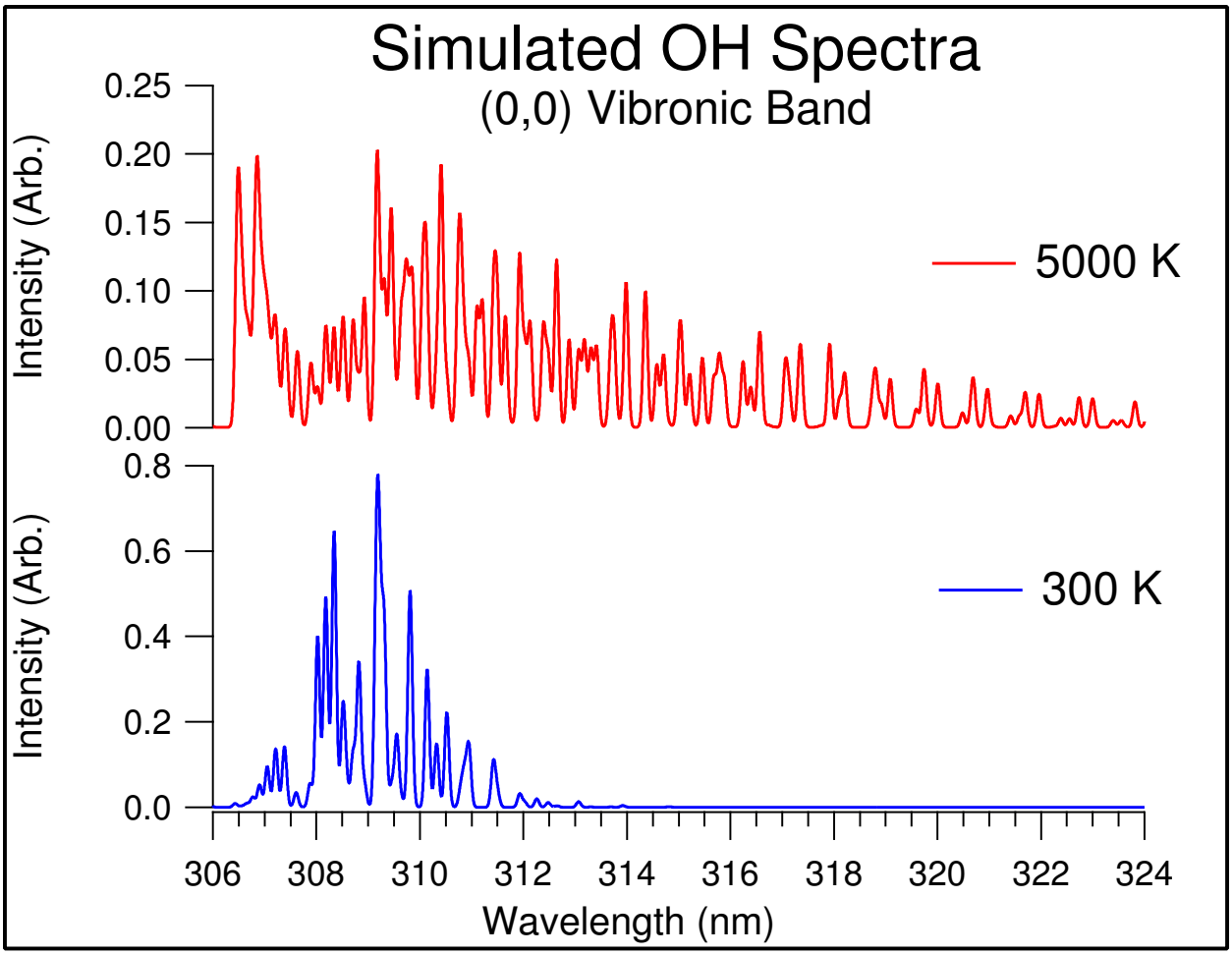

Figure 4: Simulation of A-X transition of OH at 300 K and 5000K generated with PGOPHER [16].

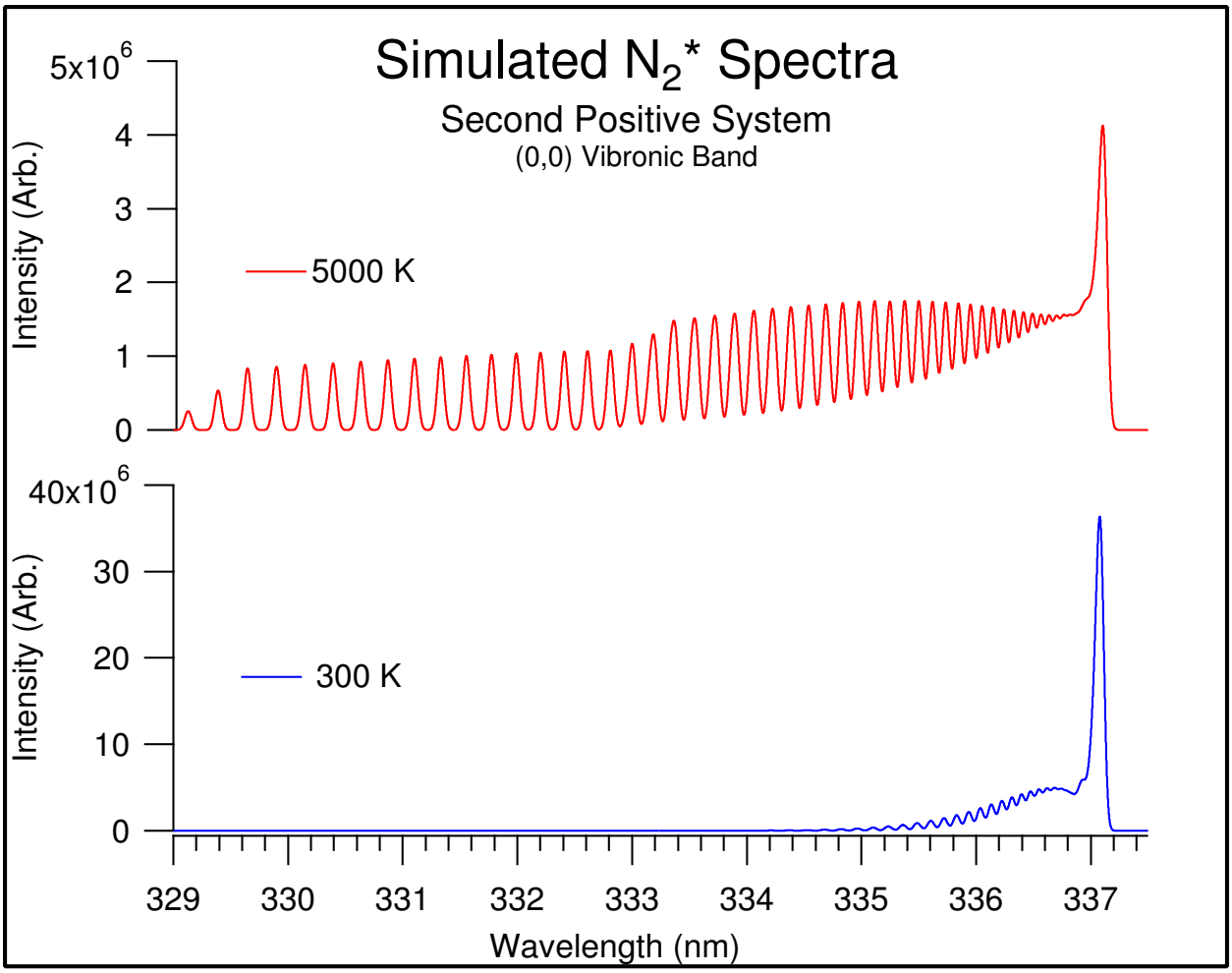

Figure 5: Simulated spectra of N_2* at room temperature and 5000 K generated using PGOPHER [16].

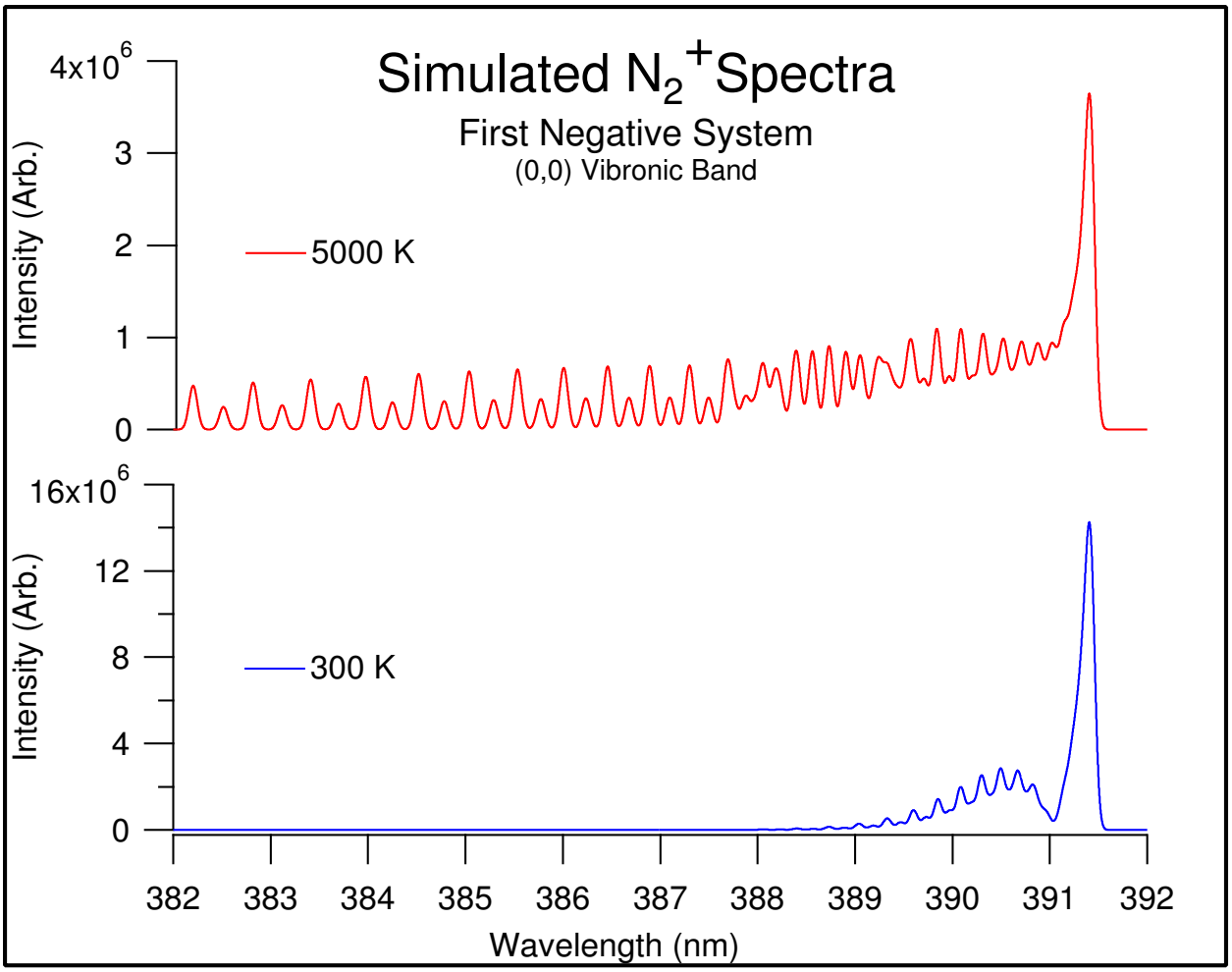

Figure 6: Simulated spectra of N_2^+ at room temperature and 5000 K generated using PGOPHER [16].

International Journal of Mass Spectrometry 376 (2015) 39–45

Contents lists available at ScienceDirect

International Journal of Mass Spectrometry

journal homepage: www.elsevier.com/locate/ijms

Mass spectrometry of atmospheric-pressure ball plasmoids

Scott E. Dubowsky, David M. Friday, Kevin C. Peters, Zhangji Zhao, Richard H. Perry, Benjamin J. McCall*

Department of Chemistry, The University of Illinois at Urbana-Champaign, 600 S. Mathews Ave., Urbana, IL 61820, USA

ARTICLE INFO

Article history:
Received 6 October 2014
Accepted 22 November 2014
Available online 6 December 2014

Keywords:
Plasma
Plasmoid
Mass spectrometry
Ambient ionization
Ball lightning

ABSTRACT

Ball lightning is a naturally occurring atmospheric event that has perplexed researchers for centuries, and there is to date no complete explanation (chemical, physical, or otherwise) as to why ball lightning behaves the way that it does. There has been considerable effort to try to both produce and measure the properties of ball lightning type discharges over recent years, and this collected work has begun to reveal some interesting physical and chemical phenomena. We are able to produce water-based plasma ball discharges using high-voltage equipment, and these self-contained plasmoids are considered to be similar to natural ball lightning. In this article we present the first mass spectrometric analysis of water-based ambient ball plasmoids. Using an extremely simple sampling technique, we were able to detect several chemical species within the interior of the plasmoid. Several molecules that are common to plasmas generated in air were observed in the mass spectra, such as $[NO_2]^+$ and $[NO_3]^+$. More interestingly, we observed the protonated water clusters $[(H_2O)_2H]^+$ and $[(H_2O)_3H]^+$, ammonia (NH_3) as a component of a copper cluster, and several anions. Furthermore, many species observed in the mass spectra are in the form of hydrated clusters.

© 2014 Elsevier B.V. All rights reserved.

1. Introduction

Ball lightning is a one-in-a-million [1] atmospheric phenomenon that is poorly understood due to its rarity and unpredictability. Eyewitness accounts across several centuries describe large balls of light moving across the sky for several seconds during thunderstorms, with some reports detailing powerful explosions occurring when the ball of light dissipates. Images and video recordings of ball lightning phenomena have been captured by amateurs and are readily available via an internet search, however it was only last year that the first scientific measurements and analysis of naturally-occurring ball lightning were reported [2]. Cen et al. set out to observe cloud-to-ground lightning strikes during a thunderstorm in China's Qinghai Plateau, and by a brilliant stroke of luck ball lighting was observed immediately after a cloud-to-ground lightning strike. Their observation site was 0.9 km from the site of the ball lightning, which had a reported lifetime of 1.64 s and a diameter of approximately 1.1 m. The ball lightning event was characterized using emission spectroscopy, and emission lines from components of soil (iron, silicon, calcium, nitrogen) were observed in the spectra [2].

There is some debate in the literature regarding plausible theories that explain the properties of ball lightning [3–8], and to date there is no concrete physical or chemical explanation as to how ball lightning is formed and how these spheres of plasma can last for an extended period of time without energy input from an external power source. Perhaps the most fascinating aspect of ball lightning is this extended lifetime. It is remarkable that at atmospheric pressure and temperature, self-sustaining plasmas can last for more than a second. Simulations which model upwards of 600 chemical processes that could occur in ambient plasma discharges show that most reactions within this type of plasma should be complete in a millisecond or less [9,10], however ball lightning seems to defy the current understanding of atmospheric-pressure plasmas. Given the complexity of the system in question, a true phenomenological explanation of the formation mechanism and lifetime of ball lightning will most likely be a combination of several different physical and chemical processes.

In order to truly answer the fundamental questions surrounding the long lifetime of ball lightning, it is essential to generate plasmas that are at the very least semi-analogous to natural ball lightning. Tesla was the first to observe a "fireball" type discharge [11], and efforts to reproduce his experiments have led to direct current (DC) electrical discharges that can produce plasmas similar to ball lightning. Traditionally, DC plasma generating apparatus produce arc, corona, glow, or dielectric barrier discharges between

* Corresponding author. Tel.: +1 2172440230.
E-mail address: bjmccall@illinois.edu (B.J. McCall).

http://dx.doi.org/10.1016/j.ijms.2014.11.011
1387-3806/© 2014 Elsevier B.V. All rights reserved.

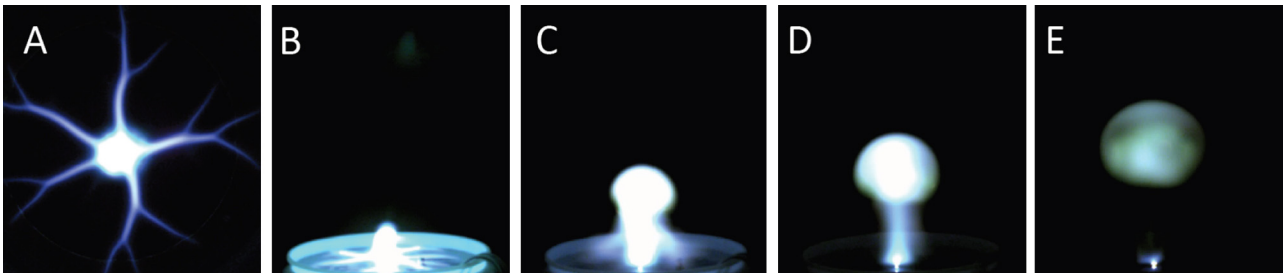

Fig. 1. Images of a plasmoid discharge from start to finish. (A and B) Pre-initiation phase, (C and D) buildup phase, (E) detachment phase. (B–E) were obtained from a single discharge via high-speed videography (Pixelink® PL-B&42U. (A) was obtained from a separate discharge under identical conditions, top–down camera setup.

two electrodes at atmospheric pressure [12]. These discharges are usually well behaved and are easily characterized with a variety of diagnostic techniques [13,14].

Additionally, ambient DC plasmas have been thoroughly characterized by mass spectrometry (MS) due to their use as ionization sources [15,16]. If the electrode configuration is such that it allows for the plasma to form and grow in one place, a free-floating and self-sustaining plasma can be produced. Since these self-contained plasmas last for an extended period of time with no external source of energy they are referred to as "plasmoids."

Using a water-based technique, Egorov and Stepanov were the first to produce a plasmoid discharge of this type in a laboratory [17], and several other groups have produced discharges similar to what they described [18–20]. To summarize this work, a bank of large capacitors was charged to several kV, and using high-voltage switches a short pulse of current was applied across two electrodes, one of which was fully submerged in a container full of water. The other electrode (the cathode in this case) was positioned such that just the tip slightly protruded from the surface of the water in the bucket. A plasmoid began to form, and buoyant forces generated from local heating of the ambient air around the tip of the cathode caused the plasmoid to rise upward and away from the tip of the cathode.

There are three distinct phases to this type of plasmoid formation (Fig. 1): the pre-initiation, buildup, and detachment phases [21]. First, current begins to flow from one electrode to the other, and "streamers" or "spider legs" begin to form and extend over the surface of the water rather than through the bulk electrolyte solution. In the center, above the cathode, a small ball of plasma begins to form. Next, the ball of plasma begins to grow in size and rise due to buoyant forces while still receiving continuous current from the cathode. Finally, when the capacitor has discharged a sufficient amount of energy, no additional plasma is formed, and a self-sustaining plasmoid remains for an extended period of time. In other words, the energy stored in the capacitor at the end of a discharge event is not sufficient to allow for additional plasmoid formation. Using our experimental setup, the detachment phase can last up to 200 ms, with an entire discharge event (pre-initiation, buildup, and detachment phases) lasting up to 400 ms.

Versteegh et al. have provided the most detailed insight into the underlying chemistry and physics of water-based plasmoid discharges using emission spectroscopy and probe measurements [19]. In this work, emission lines from H, Na(I), Ca(I), Ca(II), Cu(I), OH radical, and CaOH were observed in the ultraviolet/visible. Along with qualitative identification of chemical species present within the plasmoid, these specific emission lines reveal that the electron temperature of the discharge cannot be very high (< 1 eV), otherwise emission lines from more highly energetic atoms and molecules would have been observed. Furthermore, intensity ratios of a pair of Ca(I) lines were used to estimate the electron temperature to be 5000 K (0.43 eV) at the time of the initial pulse and 2500 K (0.22 eV) after 225 ms. Further investigation into the rotational temperature of the hydroxyl radical showed a non-thermal distribution of temperatures, leading to the hypothesis that the products of water dissociation contain the necessary energy to sustain visible emission for an extended period of time. Additionally, Stark broadening of Cu(I) lines in the pre-initiation phase of the discharge was used to estimate electron densities in the plasma to be on the order of 10^{16} cm^{-3} at 10 ms and 10^{14} cm^{-3} at 75 ms.

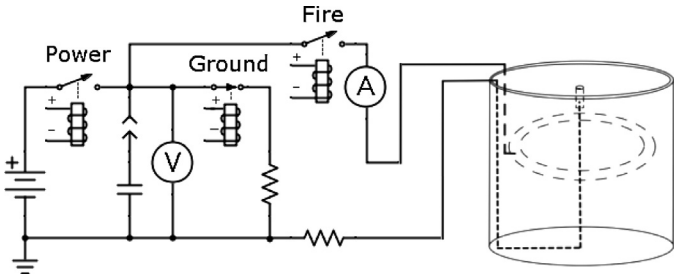

Fig. 2. Circuit diagram of plasmoid generating apparatus. *V* is a voltage divider across which voltage measurements are taken, *A* is a Hall effect current sensor.

2. Experimental

2.1. Plasmoid generator

The equipment that we use in our laboratory has been described previously [22], but some of the key components will be highlighted here for the sake of clarity and understanding. Our power supply can produce up to ±10 kV DC and wiring our capacitors in parallel can generate greater than mF capacitances, thereby generating several kJ of energy. A schematic of the hardware and circuitry is shown in Fig. 2. The following description of the experimental setup was the same for every trial unless specifically noted otherwise. Voltage and capacitance parameters were chosen in part because of safety concerns, but discharges under these conditions are typically well behaved. It is also important to mention that, much like natural lightning strikes, no two plasmoid discharges are exactly alike. In other words, under identical conditions the lifetime, shape, rise velocity, and electrical behavior of plasmoid discharges can vary.

An 873 μF parallel-plate, oil-filled capacitor (Maxwell) was charged to +4000 V DC using a Glassman EK Series high-voltage power supply. The current being transferred from the capacitor to the plasmoid generator and eventually to ground was regulated by a series of three Ross Engineering high-voltage E Series relays. An Arduino® Uno microcontroller controlled the timing of these relays and recorded current and voltage measurements. Current pulses were applied across two electrodes, one of which was fully submerged in a very dilute solution of hydrochloric acid in water, a more detailed description of which is given in the next section. One full plasmoid discharge will also be referred to as a "shot" at other points in this article.

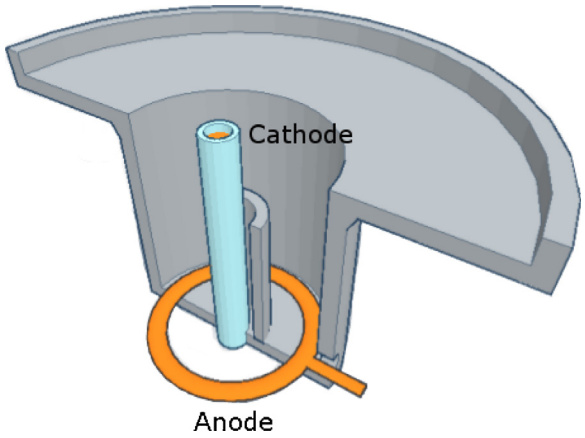

Fig. 3. Schematic depicting a cross-section of the "bowl" plasmoid generator.

2.2. Electrode materials and discharge containers

Some of the properties of the physical apparatus were changed for different sets of experiments, namely the electrode material and size of the container in which the electrodes were submerged. The fill solution for the discharge containers was prepared with either deionized water or D_2O and concentrated HCl. The vessel would be filled with deionized water or D_2O, and HCl would be added dropwise until the desired conductivity of the solution was reached. Conductivity measurements were taken with a handheld meter (Oakton PCSTest^{TM}35). For this set of experiments, the conductivity was set to 200 μSiemen.

The cathodes for these experiments consisted of either a solid copper rod or a solid tungsten rod, each with a six mm diameter. The electrode was insulated from the surrounding aqueous environment with a piece of alumina tubing having an inner diameter of 6 mm and an outer diameter of 8 mm. This was done in order to electrically isolate the cathode from the water, in other words to ensure that current would travel above the surface of the water. Copper was chosen for two reasons: the distribution of the naturally occurring isotopes (^{63}Cu and ^{65}Cu) is well known and easily observed via MS, and copper ionizes easily, allowing for the formation of small cluster ions around a metallic center. Tungsten was chosen because it is extremely robust and can stand up to repeated trials with minimal degradation, therefore no tungsten ions were observed in any MS experiments, making it an ideal cathode for deuterium substitution experiments where we wanted to minimize the interaction of metal ions with water clusters and other ions.

Two different containers were used in this work, the first being a store-bought polyethylene five-gallon bucket, the second being a custom acrylonitrile butadiene styrene (ABS) plastic bowl (Fig. 3) with a fill volume of approximately 200 mL. The plastic bowl was printed using an AirWolf 3D XL printer. The exact dimensions of the electrodes within the five gallon bucket have been described previously [22], and we made no deviations in setting up this container. The dimensions of the bowl however are different in the following ways: the surface of the electrolyte is formed by the top portion of the bowl which has a diameter of 12 cm and a lip depth of 1 cm. Additionally, the anode is positioned 6 cm below the tip of the cathode and the diameter of this lower portion of the bowl is 4.5 cm. The lip at the top of the bowl provides a significant surface area of electrolyte over which plasmoid formation can occur. The anode used in the bowl was considerably smaller than the anode used in the bucket, and was constructed using thick copper wire rather than a solid ring. The wire was bent into a circle with an outer diameter of 4.5 cm, and was positioned at the bottom of the bowl. The other major advantage to using this bowl was the reduced volume required to perform discharges; this allowed for discharges over solutions in D_2O.

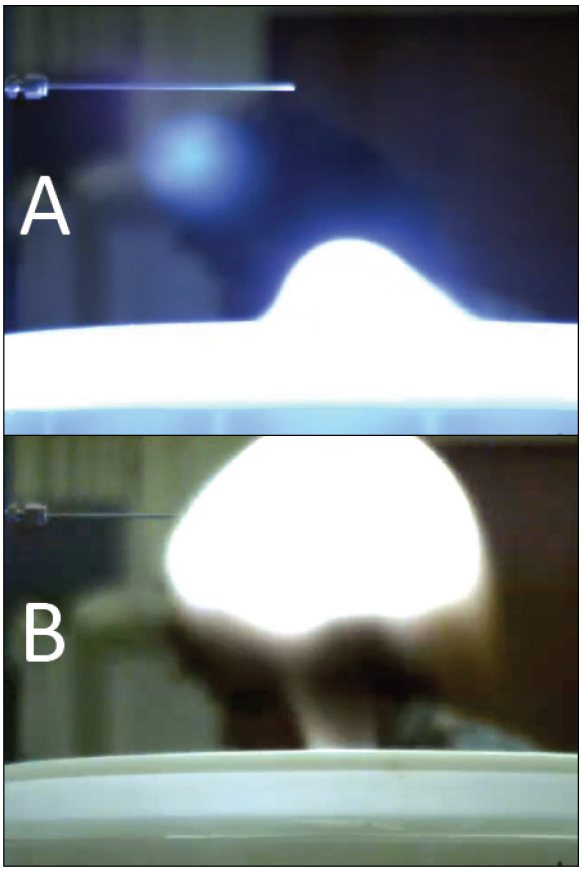

Fig. 4. Images of the stainless steel capillary relative to the position of the plasmoid discharge. (A) The pre-initiation phase and (B) the detachment phase.

2.3. Mass spectrometer and sampling

This work was performed with a Thermo Scientific LTQ-Orbitrap XL mass spectrometer, using both an ion trap and an Orbitrap for analysis of plasmoid composition. The ion trap was operated in low mass mode with a range of m/z 15–200 and at a pressure of 10^{-5} Torr, and the Orbitrap had a mass detection range of m/z 50–2000 (<5 ppm mass accuracy) with a mass resolution of 100 000, and was operated at approximately 8×10^{-10} Torr. The ion trap and Orbitrap have temporal resolutions of 60 and 600 ms per scan, respectively [23].

The sampling technique was extremely simplistic in order to avoid adding or removing ions or chemical species to or from the plasmoid discharge. A stainless steel capillary (Fig. 4) with a length of 30 cm and an inner diameter of 0.8 mm was held at a potential of ±35 V and was positioned 8 cm above the tip of the cathode. It is important to note that the images shown in Fig. 4 were obtained from one shot, and the only thing that is changing position in those images is the plasmoid itself. Fig. 4A shows the position of the capillary relative to the plasmoid generator, and Fig. 4B shows that as the plasmoid rises the geometry of the setup allows the capillary to sample from within the plasmoid.

The pressure differential between the ambient environment and the inlet to the mass spectrometer was sufficient to draw the contents of the plasmoid into the instrument for analysis with appreciable signal. No additional ionization of the plasmoid contents was performed. As a result of the temporal resolution

Table 1
Singly charged copper based ions observed in plasmoid discharges.

Ion	Average ion fraction	Average deviation	Mass accuracy (ppm)
$[Cu]^+$	0.02	±0.01	1
$[Cu\ NH_3]^+$	0.03	±0.01	2
$[Cu\ H_2O]^+$	0.14	±0.06	3
$[Cu\ (NH_3)_2]^+$	0.006	±0.004	4
$[Cu\ NH_3\ H_2O]^+$	0.04	±0.02	1
$[Cu\ (H_2O)_2]^+$	0.14	±0.07	4
$[Cu(CH_3CN)]^+$	0.09	±0.06	4

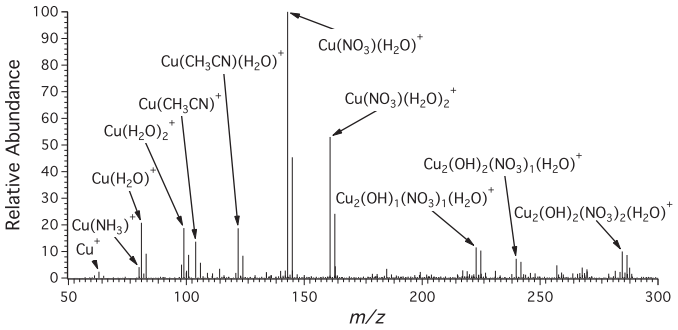

Fig. 5. An example Orbitrap mass spectrum of a plasmoid generated with a copper electrode over a solution of water. The labels indicate only ^{63}Cu-containing ions.

of the different traps, several mass spectra were obtained for one plasmoid discharge event, and averaging these spectra provided a comprehensive survey of the internal composition of the plasmoid over a complete shot.

3. Results and discussion

3.1. Orbitrap MS

The mass spectra obtained when using a copper cathode and the Orbitrap mass analyzer showed consistent signals from several singly charged ions, a summary of which is given in Table 1. Fig. 5 shows a representative mass spectrum obtained when using the Orbitrap, and shows more than a dozen resolved signals. Average ion fractions were obtained by dividing the raw intensity of the signal by the total raw intensity. The deviations in ion fraction were taken across seven trials for all ions except $[Cu(CH_3CN)]^+$, the deviation of which was taken across three trials. Mass accuracies are reported in parts per million. All of the spectra described in this article were externally calibrated using the signal from $[^{63}Cu]^+$.

The first trend that can be observed in these spectra is the presence of copper clusters. This presence of copper ions was a result of using a copper cathode for this set of experiments. Fig. 5 also shows signals from both isotopes of copper (only ^{63}Cu cluster ions are labeled on the spectrum). On closer inspection, ^{65}Cu clusters containing the same ligands can be assigned using the expected mass differences, and the ratio of intensities between the ^{63}Cu and ^{65}Cu clusters corresponds to the natural abundances of the copper isotopes. Additionally, water was also a component of many ions in the collected spectra. There are two plausible ways in which water could be associated with the plasmoid. First, water can be pulled up into the plasmoid from the electrolyte solution contained within the bucket due to the intense localized heating at the tip of the electrode. Second, water could associate with the plasmoid through humidity in the surrounding air. How water associates with the plasmoid is not entirely obvious, however this will be discussed later in the article.

The presence of ammonia in the interior of the plasmoid is also significant: to our knowledge, this is the first observation of

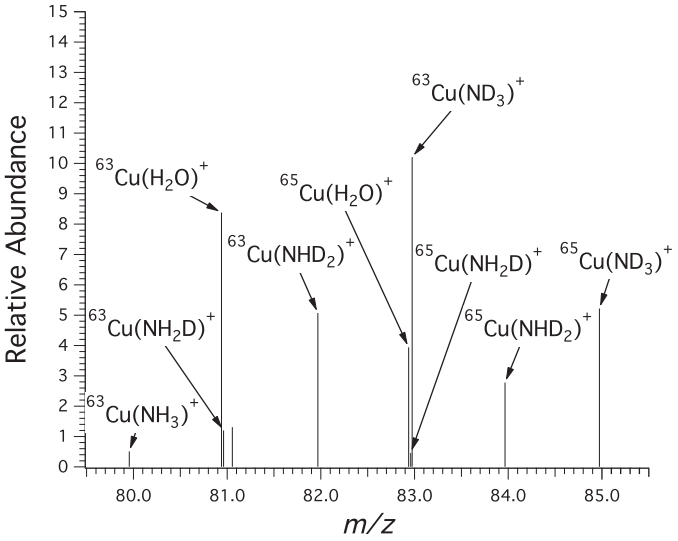

Fig. 6. Portion of an Orbitrap mass spectrum of a plasmoid discharge using a copper cathode above a solution of D_2O showing deuteration of ammonia. Ions containing both copper isotopes are labeled accordingly.

Table 2
Singly charged, low mass ions observed in the ion trap.

Ion	Average ion fraction	Average deviation	Mass accuracy (ppt)
$[NO]^+$	0.05	±0.03	4
$[H(H_2O)_2]^+$	0.13	±0.05	5
$[NO(H_2O)]^+$	0.12	±0.06	3
$[H(H_2O)_3]^+$	0.1	±0.04	3

ammonia in an ambient, water-based plasmoid discharge. To determine whether the presence of ammonia as a ligand was a result of ammonia molecules from the ambient air interacting with copper ions or if in fact ammonia is formed in the process of plasmoid formation, discharges were performed over a heavy water solution. Fig. 6 shows the expected mass shifts for each isotopologue of the $[Cu(NH_3)]^+$ ion. This indicates that ammonia is formed as a product during a plasmoid discharge.

3.2. Ion trap MS

Although the Orbitrap has a much higher mass resolution than the ion trap, many low mass (m/z <50) ions that were suspected to be in the interior of plasmoid were not detected in the Orbitrap. This was especially important in the search for protonated water clusters, the protonated dimer and trimer having molecular weights of m/z 37 and m/z 55, respectively. Therefore we performed IT-MS scans of individual plasmoid discharges, all of which reveal a consistent pattern of signals generated by small singly-charged ions, a list of which is provided in Table 2. Ion fractions were calculated by dividing the raw intensity of the signal by the total raw intensity. The deviations in ion fraction were taken across six trials for all ions. The mass accuracy is reported in parts per thousand.

Fig. 7 shows two examples of ion trap spectra. The resolution is notably lower, however the signal-to-noise ratios of the signals were significant enough to allow assignment of low molecular weight ions. It is important to note that in Fig. 7B the deionized water-based electrolyte was changed to a heavy water based electrolyte with the same concentration of HCl. Each signal from water-containing ions within the plasmoid had the appropriate mass shifts resulting from deuterium substitutions. An attempt was made to perform MS/MS analysis on the protonated water clusters to further confirm their identities, however no significant signals

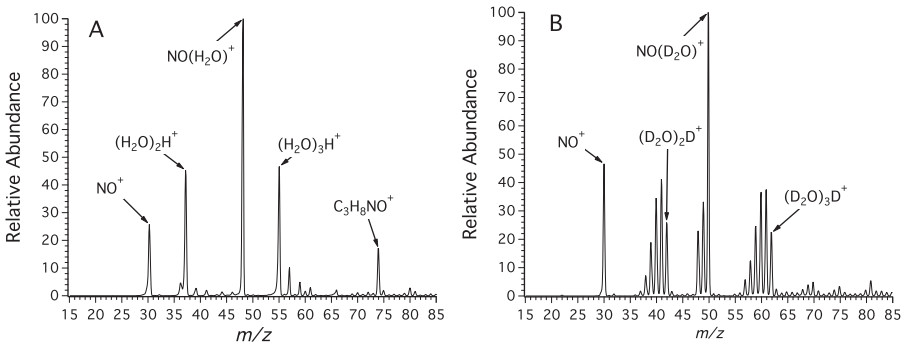

Fig. 7. Two examples of ion trap mass spectra. (A) Solution of HCl in deionized water and (B) solution of HCl in D_2O.

were observed during this set of experiments. This is most likely a result of the difficulties encountered when trying to fragment low molecular weight ions for MS/MS analysis. However, the position of the signals and the distribution patters of the clusters in the ion trap spectra are sufficient to prove the identities of the protonated water clusters.

3.3. Negative mode MS

In addition to positive mode scans we also performed negative mode scans in an effort to identify negative ions in the plasmoid. In low pressure plasma discharges, negative ions are relatively rare due to the inefficiency of radiative attachment. However the higher pressure at ambient conditions leads to more efficient production of negative ions through three-body attachment. We observed that the number density of anions is much less than that of positively charged species in the plasmoid interior: when comparing plasmoid discharges under identical conditions, we observed that the raw intensity of the positive mode signals was approximately thirty times larger than that of the negative mode signals. Several discharges were analyzed using negative mode in both the Orbitrap and the ion trap, and four negatively charged ions were observed: $[NO_2]^-$, $[NO_3]^-$, $[HN_2O_5]^-$, and $[HN_2O_6]^-$. Other than those of the nitrate anion, our observations of these ions were not entirely consistent from shot to shot. This is most likely the result of the already small number densities of anions fluctuating between discharges.

3.4. Statistical analysis of deuterated isotopes

In order to get a better sense of the chemical processes occurring during a plasmoid discharge, the distribution of deuterium within the isotopologues of the protonated water clusters was analyzed. What is readily apparent without performing any calculations is that many of the ions observed in the plasmoid are generated from the electrolyte solution in the discharge container. This can be seen in Fig. 7B, where a D_2O solution was used in place of a solution of deionized water. The signals in the ion trap spectra show that any low mass ions that contain hydrogen underwent deuterium substitution to all allowed isotopologues, however the distribution of these deuterium atoms is not readily apparent on first inspection.

We first attempted to develop a model that explained the distribution of these protonated water cluster isotopologues in the plasmoid to be a result of protons and deuterons randomly combining assuming a binomial distribution. A binomial distribution is defined as:

$$Population(k) = \binom{n}{k} P_D{}^k (1 - P_D)^{n-k} \quad (1)$$

where population refers to the fractional population of each isotopologue, n is the number of total number of possible substitutions that can occur for the particular cluster, k is the number of deuterium substitutions that have occurred for the particular isotopologue, and P_D is the fraction of hydrogen atoms in the form of deuterium: $P_D = n_D/(n_D + n_H)$. We found that it was not possible to fit the observations with this model for any value of P_D. This model assumes that the clusters were formed from individual hydrogen and deuterium atoms, which is not physically accurate for this system, so the failure of this simple model may not be too surprising.

A two-parameter model of a binomial distribution of water clusters was then created using the following relationship:

$$Pop.(k_1, k_2) = \binom{n_1}{k_1} P_{D_2O}{}^{k_1} (1 - P_{D_2O})^{k_1 - n_1} \times \binom{n_2}{k_2} P_D{}^{k_2} (1 - P_D)^{k_2 - n_2} \quad (2)$$

where n_1 and n_2 are the total number of H_2O/D_2O molecules and H^+/D^+ ions in each cluster ($n_1 = 2$ *or* 3, $n_2 = 1$ in all cases), k_1 and k_2 are the number of deuterated species of each form (D_2O and D^+), and P_{D_2O} and P_D are the fractions of water molecules and protons in deuterated forms from which the clusters are presumed to be formed.

This new model assumes that clusters are formed from water molecules (H_2O or D_2O) from the electrolyte and/or ambient air, along with protons (H^+ or D^+) produced from a potentially different isotopic distribution of water. Models of this two-parameter distribution for both the protonated water dimer and trimer are shown in Fig. 8. The two clusters were analyzed independent of other ions present in the plasmoid, and the average fractional populations of each signal across four mass spectra are shown in Fig. 8. The error bars on the experimental data represent three standard deviations across the four shots, and are quite large due to the shot to shot variability described above.

Using Eq. (2) as a model, the available fractional amounts of D_2O and deuterium were varied and fit to the experimental data using a simultaneous fitting procedure. The optimized values of P_{D2O} and P_D were calculated to be 0.66 ± 0.04 and 0.47 ± 0.07 over a 95 % confidence interval, respectively. This model offers a fairly satisfactory fit to the experimental data, given the shot-to-shot variability represented in the error bars.

Within the context of this model, it is apparent that the mixing of atoms in the plasmoid is not entirely random. The water molecules within the clusters, which could conceivably originate exclusively from the electrolyte or from the ambient air, appear to come from both sources, with a slightly higher preponderance of D_2O from the electrolyte. The slightly lower value of P_D compared

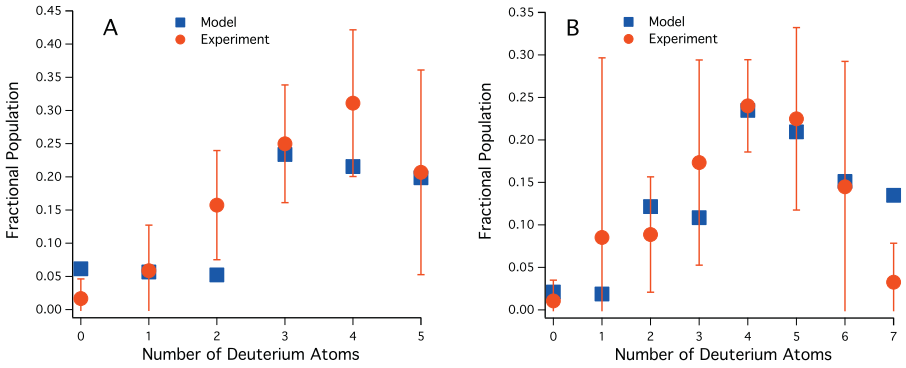

Fig. 8. Comparison of statistical model described by Eq. (2) to the experimental distributions of deuterated water clusters, (A) protonated water dimer, (B) protonated water trimer, $P_{D_2O} = 0.66 \pm 0.04$ and $P_D = 0.47 \pm 0.07$. The error bars represent three standard deviations.

with P_{D_2O} is intriguing, and suggests that protonation of water clusters might occur at later stages of the plasmoid, after more H_2O from the ambient air has been incorporated. If the reproducibility of the plasmoids can be improved, it may be possible to better constrain the chemical formation of these water cluster ions. However, at this point the observations conclusively demonstrate that plasmoid composition is not determined exclusively by the electrolyte composition.

4. Conclusions

In this article we have presented the first chemical analysis of plasmoid discharges using mass spectrometry. The simplicity of the sampling technique allowed for a qualitative survey of some of the ions that are formed in or contained by this particular type of plasmoid discharge. The statistical model that we present shows that a two-parameter binomial distribution can be used to describe the distribution of hydrogen and deuterium atoms in small protonated water clusters. Additionally, this model shows that ambient plasmoids are composed of molecules from both the electrolyte and the surrounding environment. Finally, the types of ions observed in the mass spectra, namely water clusters and NO_x species, are in agreement with what has been observed in other DC plasma discharges by MS [15,16].

The reproducibility of plasmoid discharges presents the greatest obstacle toward a true physical understanding of plasmoid stability. Efforts are underway to improve the hardware and control electronics that are used to generate laboratory plasmoids. Further characterization of plasmoids, both by MS and by spectroscopic and imaging methods, can be expected to provide additional information about the composition and dynamics in these fascinating objects that may ultimately lead to an understanding of their chemical and physical properties.

Acknowledgements

We would like to thank C. Michael Lindsay for his continuing advice and encouragement, as well as for securing the equipment described in this article. S.E.D. would also like to thank other members of the Perry research group for constructive and helpful discussions.

References

[1] D. ter Haar, An electrostatic-chemical model of ball lightning, Phys. Scr. 39 (6) (1989) 735 http://stacks.iop.org/1402-4896/39/i=6/a=010
[2] J. Cen, P. Yuan, S. Xue, Observation of the optical and spectral characteristics of ball lightning, Phys. Rev. Lett. 112 (2014) 035001, http://dx.doi.org/10.1103/PhysRevLett.112.035001.
[3] J. Abrahamson, Ball lightning from atmospheric discharges via metal nanosphere oxidation: from soils, wood or metals, Philos. Trans. R. Soc. Lond. Ser. A: Math. Phys. Eng. Sci. 360 (1790) (2002) 61–88, http://dx.doi.org/10.1098/rsta.2001.0919, arXiv:http://rsta.royalsocietypublishing.org/content/360/1790/61.full.pdf+html, http://rsta.royalsocietypublishing.org/content/360/1790/61.abstract
[4] J.M. Donoso, J.L. Trueba, A.F. Rañada, The riddle of ball lightning: a review, Sci. World J. 6 (2006) 254–278, http://dx.doi.org/10.1100/tsw.2006.48.
[5] K.D. Stephan, Electrostatic charge bounds for ball lightning models, Phys. Scr. 77 (3) (2008) 035504 http://stacks.iop.org/1402-4896/77/i=3/a=035504
[6] A. Shavlov, The two-temperature plasma model of a fireball. The calculated parameters, Phys. Lett. A 373 (43) (2009) 3959–3964, http://dx.doi.org/10.1016/j.physleta.2009.08.060 http://www.sciencedirect.com/science/article/pii/S0375960109010871
[7] K. Tennakone, Stable spherically symmetric static charge separated configurations in the atmosphere: Implications on ball lightning and earthquake lights, J. Electrostat. 69 (6) (2011) 638–640, http://dx.doi.org/10.1016/j.elstat.2011.08.005 http://www.sciencedirect.com/science/article/pii/S0304388611001495
[8] S. Shevkunov, Cluster mechanism of the energy accumulation in a ball electric discharge, Doklady Phys. 46 (7) (2001) 467–472, http://dx.doi.org/10.1134/1.1390398.
[9] P. Xuexia, D. Zechao, J. Pengying, L. Weihua, L. Xia, Influence of ionization degrees on the evolutions of charged particles in atmospheric plasma at low altitude, Plasma Sci. Technol. 14 (8) (2012) 716 http://stacks.iop.org/1009-0630/14/i=8/a=07
[10] Y. Sakiyama, D.B. Graves, H.-W. Chang, T. Shimizu, G.E. Morfill, Plasma chemistry model of surface microdischarge in humid air and dynamics of reactive neutral species, J. Phys. D: Appl. Phys. 45 (42) (2012) 425201 http://stacks.iop.org/0022-3727/45/i=42/a=425201
[11] N. Tesla, Colorado Springs Notes: 1899–1900, Nolit, Beograd, Yugoslavia, 1978.
[12] C. Tendero, C. Tixier, P. Tristant, J. Desmaison, P. Leprince, Atmospheric pressure plasmas: a review, Spectrochim. Acta B: At. Spectrosc. 61 (1) (2006) 2–30, http://dx.doi.org/10.1016/j.sab.2005.10.003 http://www.sciencedirect.com/science/article/pii/S0584854705002843
[13] A. Fridman, L.A. Kennedy, Plasma Physics and Engineering, 2nd ed., CRC Press, Boca Raton, 2011.
[14] M.A. Lieberman, A.J. Lichtenberg, Principles of Plasma Discharges and Materials Processing, 2nd ed., Wiley, Hoboken, 2005.
[15] J. Shelley, J. Wiley, G. Chan, G. Schilling, S. Ray, G. Hieftje, Characterization of direct-current atmospheric-pressure discharges useful for ambient desorption/ionization mass spectrometry, J. Am. Soc. Mass Spectrom. 20 (5) (2009) 837–844, http://dx.doi.org/10.1016/j.jasms.2008.12.020.
[16] F.J. Andrade, J.T. Shelley, W.C. Wetzel, M.R. Webb, G. Gamez, S.J. Ray, G.M. Hieftje, Atmospheric pressure chemical ionization source. 1. Ionization of compounds in the gas phase, Anal. Chem. 80 (8) (2008) 2646–2653, http://dx.doi.org/10.1021/ac800156y, pMID: 18345693. arXiv:http://dx.doi.org/10.1021/ac800156y.
[17] A. Egorov, S. Stepanov, Long-lived plasmoids produced in humid air as analogues of ball lightning, Tech. Phys. 47 (12) (2002) 1584–1586, http://dx.doi.org/10.1134/1.1529952.
[18] N. Hayashi, H. Satomi, T. Kajiwara, T. Tanabe, Properties of ball lightning generated by a pulsed discharge on surface of an electrolyte in the atmosphere, IEEJ Trans. Electr. Electron. Eng. 3 (6) (2008) 731–733, http://dx.doi.org/10.1002/tee.20336.
[19] A. Versteegh, K. Behringer, U. Fantz, G. Fussmann, B. Jüttner, S. Noack, Long-living plasmoids from an atmospheric water discharge, Plasma Sources Sci. Technol. 17 (2) (2008) 024014 http://stacks.iop.org/0963-0252/17/i=2/a=024014

[20] Y. Sakawa, K. Sugiyama, T. Tanabe, R. More, Fireball generation in a water discharge, Plasma Fusion Res. 1 (2006) 39-039, http://dx.doi.org/10.1585/pfr.1.039.
[21] K.D. Stephan, S. Dumas, L. Komala-Noor, J. McMinn, Initiation growth and plasma characteristics of 'gatchina' water plasmoids, Plasma Sources Sci. Technol. 22 (2) (2013) 025018 http://stacks.iop.org/0963-0252/22/i=2/a=025018
[22] D.M. Friday, P.B. Broughton, T.A. Lee, G.A. Schutz, J.N. Betz, C.M. Lindsay, Further insight into the nature of ball-lightning-like atmospheric pressure plasmoids, J. Phys. Chem. A 117 (39) (2013) 9931–9940, http://dx.doi.org/10.1021/jp400001y, arXiv:http://pubs.acs.org/doi/pdf/10.1021/jp400001y.
[23] R.H. Perry, R.G. Cooks, R.J. Noll, Orbitrap mass spectrometry: instrumentation, ion motion and applications, Mass Spectrom. Rev. 27 (6) (2008) 661–699, http://dx.doi.org/10.1002/mas.20186.

Journal of Molecular Spectroscopy 322 (2016) 1–8

Contents lists available at ScienceDirect

Journal of Molecular Spectroscopy

journal homepage: www.elsevier.com/locate/jms

Rao Prize article

Infrared emission spectroscopy of atmospheric-pressure ball plasmoids ☆

Scott E. Dubowsky [a], Bradley Deutsch [b], Rohit Bhargava [b], Benjamin J. McCall [c,*]

[a] Department of Chemistry, University of Illinois, Urbana, IL 61801, USA
[b] Department of Chemical and Biomolecular Engineering, University of Illinois, Urbana, IL 61801, USA
[c] Departments of Chemistry and Astronomy, University of Illinois, Urbana, IL 61801, USA

ARTICLE INFO

Article history:
Received 29 September 2015
In revised form 30 January 2016
Accepted 5 February 2016
Available online 9 February 2016

Keywords:
Plasmoid
Plasma diagnostics
Rotational temperature
Infrared emission spectroscopy PGOPHER
Ball lightning

ABSTRACT

We report the first (to our knowledge) infrared emission spectra collected from water-based laboratory ball plasmoid discharges. A "ball plasmoid" results from a unique type of pulsed DC plasma discharge in which a sphere of plasma is seen to grow and eventually separate from a central electrode and last for a few hundred milliseconds without an external power source before dissipating. Typical recombination rates for plasmas at ambient conditions are on the order of a millisecond or less, however ball plasmoids have been observed to last a few hundred milliseconds, and there is no explanation in the literature that fully accounts for this large discrepancy in lifetime. The spectra are dominated by emission from water and from hydroxyl radical; PGOPHER was used to fit the experimental spectra to extract rotational temperatures for these molecules. The temperatures of the bending and stretching modes of H_2O were determined to be 1900 ± 300 K and 2400 ± 400 K, respectively and the rotational temperature of OH was found to be 9200 ± 1500 K.

© 2016 Elsevier Inc. All rights reserved.

1. Introduction

Low-temperature and atmospheric-pressure plasmas have developed as essential tools across several industries over the past few decades. The tunability of plasma discharge parameters allows for the selection of chemically and physically reactive components of the ionized medium, and operating a discharge at ambient pressures fosters numerous applications of plasmas in different settings. For example, the electron density and temperature, identities and number densities of reactive ions and radicals, UV photon flux, and flow rate of gases can all be tuned and optimized for interactions with different surfaces ranging from plastics to human teeth to the top layers of the skin. There has been much development of plasmas as tools for semiconductor processing [1,2], medicine [3–5], dentistry [6], air purification [7], wastewater [8] and biomedical [9–13] sterilization, as agents for controlled mutagenesis [14], and in the food processing and sterilization industry [15,16]. Additionally, ambient plasmas are attractive as soft ionization sources for mass spectrometry [17–19], especially due to the much less complicated sample preparation required for ambient ionization using plasmas.

Plasmas that are self-sustaining and have a definitive shape but are not confined between two electrodes or any external fields are referred to as plasmoids. A several-kilovolt capacitive discharge above the surface of a weak electrolyte can be used to generate water-based plasmoids [20] which take the form of a sphere, thus this particular type of discharge is referred to as a "ball" plasmoid discharge. In contrast to other direct-current (DC) plasma discharges (arc, corona, glow, dielectric barrier) [21], ball plasmoid discharges are generated by intentionally designing the electrodes such that a tremendous pulse of current causes a plasma to form at the tip of the cathode, above the surface of the electrolyte [20,22–24]. While still forming, the plasma grows, rises, and eventually separates from the cathode and can be seen as a distinct sphere of plasma for an extended period of time. The discharge occurs in three phases (Fig. 1): the pre-initiation, buildup, and detachment phases [25,26]; it is perhaps the detachment portion of the discharge, when an autonomous plasmoid can be observed, that is the most interesting. Plasma discharges at ambient pressures are not expected to last for more than a millisecond without an external power source [27,28], however ball plasmoids emit light for approximately 200 ms even when no current flows between the electrodes.

☆ The article is based upon a presentation by the author at the 70th International Symposium on Molecular Spectroscopy in June 2015 at Urbana-Champaign, which was selected by the Symposium Prize Committee for the Rao Prize as one of the three best presentations by a graduate student.

* Corresponding author.
E-mail address: bjmccall@illinois.edu (B.J. McCall).

http://dx.doi.org/10.1016/j.jms.2016.02.005
0022-2852/© 2016 Elsevier Inc. All rights reserved.

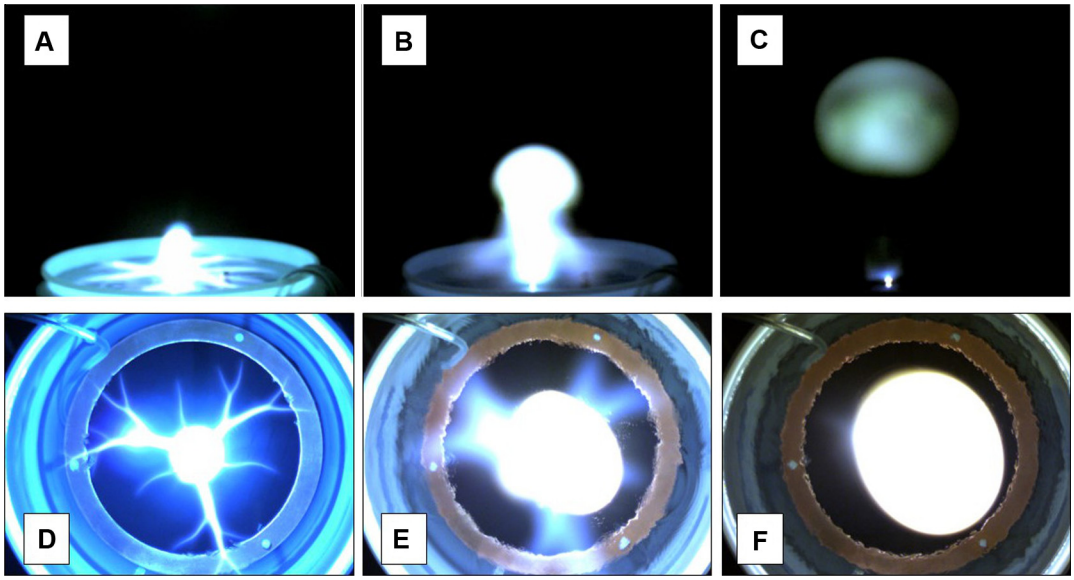

Fig. 1. Images obtained from high-speed videography of plasmoid discharges. (A–C): initiation, propagation, and detachment phases of the discharge. (D–F): top-down view of the same phases shown in A–C, taken from an identical discharge on the same day.

Recently, several groups have begun to characterize ball plasmoid discharges in attempts both to explain the long lifetime of the plasmoid and to study the mechanism of ball plasmoid formation [23,24,29,25,26], and this collection of papers has provided a foundation for more detailed studies of the system. Our goal for the experiments described in this article is twofold: to expand the emission spectroscopy performed by Versteegh et al. [23] into the infrared, and to confirm the molecular assignments obtained from infrared absorption spectroscopy presented by Friday et al. [29]. In addition to identifying the molecules which are emitting in the infrared, we aim to determine rotational temperatures for each of the emitting molecules, which will provide a more complete picture of the energy distribution of products generated during plasmoid formation and will also allow for an approximation of the gas-kinetic temperature of the plasmoid to be made.

Ball plasmoids are considered to be laboratory analogues of ball lightning, a puzzling and currently unexplained natural phenomenon which was only recently observed in the field with scientific instrumentation [30]. Although rare, there are numerous reports available in the literature describing a luminous sphere of light dancing through the sky, sometimes lasting tens of seconds before dissipating. Some reports describe a quiet fizzling out of the light, but others indicate that the ball leaves destruction in its wake as it disappears with tremendous energy. There is also debate in the literature over the theories describing the formation and other properties of ball lightning [31–35], often with little or no experimental evidence, therefore there is currently no explanation (or set of explanations) as to why ball lightning behaves in these mysterious ways.

2. Experimental

2.1. Plasmoid discharge source

The equipment and electronics that we use to generate plasmoid discharges have been described previously [29,26], however some changes have been made to the circuitry to better control and monitor the discharge. To provide as accurate a description of the apparatus as possible, the key components of the system will be described. The next paragraph describes the general process by which ball plasmoids are generated, and the following paragraphs describe additional components of the system. As is always the issue with performing these measurements, there is a high shot-to-shot variability in successive plasmoid discharges. Much in the same way that no two lightning strikes are alike, identical conditions can produce plasmoid discharges with different underlying characteristics (size, lifetime, amperage, rise velocity, etc.).

The electrode setup is contained within a store-bought five-gallon polypropylene bucket which is filled with deionized water. The conductivity of the water is adjusted using concentrated HCl. Conductivity measurements are taken with a hand-held, waterproof meter (Oakton PCSTest™35). The cathode is positioned such that just the tip of the electrode protrudes above the surface of the water approximately 1–2 mm. The cathode which is used in all of the following experiments is a solid tungsten rod with a diameter of 6 mm. The cathode is insulated from the electrolyte using a tube of alumina with an inner diameter of 6 mm and an outer diameter of 8 mm. No metal ions from the cathode were desired to be present in the discharge during these experiments, so tungsten was chosen for its high durability and resistance to sputtering and spalling. This cathode was chosen in order to minimize ion-neutral and ion–electron interactions caused solely by electrode materials, thus producing a plasmoid from only molecules in the air and molecules just above the surface of the electrolyte [26]. A copper ring is used as the anode and is positioned perpendicular to the orientation of the cathode, in other words the plane of the anode is parallel to the surface of the electrolyte. This entire electrode is submerged in the weakly conductive aqueous solution with a final depth of approximately 12 cm below the surface of the electrolyte.

Fig. 2 provides an illustration of the circuitry used in our laboratory. A Glassman EK Series high-voltage DC power supply is used to charge large parallel-plate, oil-filled capacitors (Maxwell) to 1–10 kV. The capacitors can be used individually or can be wired in parallel to generate capacitances up to two milliFarads. Three Ross Engineering E Series high-voltage relays are used to make connections that will charge the system, send current pulses to the discharge container, or ground the system. An Arduino®Uno microcontroller board controls the timing of these switches, and the same microcontroller is used to record voltage and current measurements via a voltage divider and Hall effect sensor, respectively. High-speed videography is performed with a Pixelink®PL-

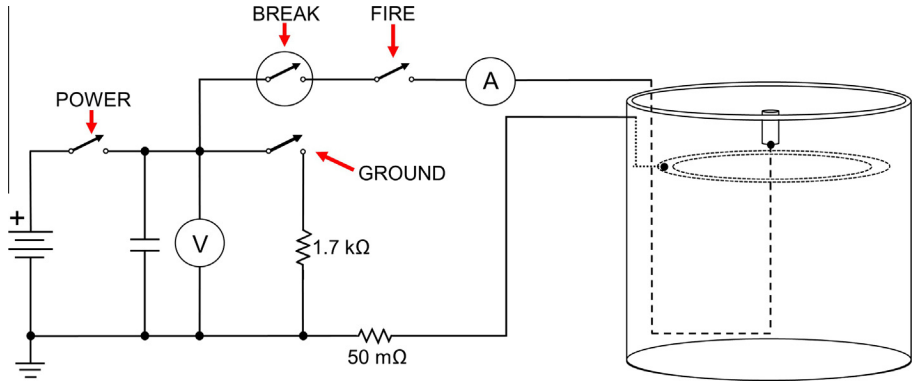

Fig. 2. A simplified circuit diagram of the plasmoid discharge circuit. The "POWER" relay delivers current to the capacitor bank, the "FIRE" relay delivers the pulse to the electrodes, "BREAK" is the vacuum relay which breaks current to the electrodes, and finally the "GROUND" relay grounds the system. V and A are a voltage divider and a Hall effect current sensor, respectively.

B&42U camera with a frame rate of 98 fps. Discharge parameters are chosen based both on the geometry of the setup and an optimization of safety to personnel and equipment, therefore no discharges above 7 kV are ever performed due to physical limitations of the equipment (temperature rating of power resistors, arcing concerns, etc.). Future additions and improvement to the circuitry will allow for larger voltages and capacitances to be used safely and successfully.

The parameters of the discharges described in this article are the following: the capacitor (873 μF) was charged to 6 kV, the conductivity of the electrolyte was set to 320 μSiemen, and the tip of the cathode was set flush to the tip of the alumina insulator which was positioned to protrude approx. 1–2 mm above the surface of the electrolyte. The conductivity of the electrolyte did not change significantly between experiments due to resistive heating. All spectra were recorded on the same day, under identical conditions.

2.2. Spectroscopic measurements

Infrared emission spectroscopy was performed using a Bruker VERTEX 70 Fourier-transform infrared spectrometer in a double-pass configuration at 4 cm^{-1} resolution and a (mirror) scan rate of 40 kHz. Spectra were collected between 1000 and 5000 cm^{-1}. The time-domain interferogram data from the spectrometer were high-pass filtered using a second-order Butterworth filter, Hanning apodized, and Hilbert transformed (phase correction) to generate emission spectra. The lineshapes in these spectra are ultimately dictated by the response function of the instrument (a Hanning function Fourier transformed to a *sinc* function in this case), thus the experimental lineshapes are best described by a Lorentzian profile with a FWHM of 4 cm^{-1}. Only one scan was used for each measurement, and it is important to note that the spectrometer and discharge electronics (each with their own small internal triggering delays) were triggered by hand. The spectrometer and discharge were triggered independently by two individuals after a countdown; no time-resolved measurements could be performed using this setup.

Fig. 3 provides a birds-eye view of the experimental setup. The HeNe laser within the instrument was used in conjunction with additional optics placed outside of the instrument to align the light emitted from the plasmoid into the spectrometer. To confirm the placement of the optics, a flame from a butane lighter was held where the plasmoid would be discharged and at points along which the emitted light was presumed to be traveling. The intensity counts on the detector were monitored in real time as the flame was brought in and out of the optical path. The intensity counts at the detector would increase by a few orders of magnitude when emitted light from the flame was detected. An opaque sheet was also placed between the plasmoid and the optics to isolate the emitted light. A hole was cut into the sheet such that the tip of the electrode was masked but the plasmoid itself was not. This eliminated the possibility of light from the hot cathode interfering with our measurements. This also minimized reflections off of other surfaces in the laboratory.

3. Results and discussion

3.1. Emission spectra

Fig. 4 shows several spectra that were obtained over the course of the experiment. A cursory examination of these data shows that water dominates the spectra, but a closer inspection shows that emission from hydroxyl radical is also present. Using the HITRAN [36] database in conjunction with the PGOPHER [37] program, a simulated mixture of these molecules was generated and compared to the experimental spectra. The simulated spectrum displayed in Fig. 4 (the uppermost spectrum) shows good agreement with the experiment in terms of the molecules that are emitting from the plasmoid.

Given that there was a significant pathlength between the plasmoid and the spectrometer in these experiments, it was necessary to account for absorption by water and CO_2 along this optical path. In order to address this issue, the observed spectra were divided by an absorbance spectrum of CO_2 and water (298 K, 2.06 m pathlength, Lorentzian lineshape; 4 cm^{-1} linewidth, 1 atm) generated using HITRAN online (http://hitran.iao.ru/). In each spectrum this resulted in a significant increase in emission signal in the regions where atmospheric CO_2 and water readily self-absorb, however there is little effect on the intensity between 2400 and 3200 cm^{-1} (where emission from OH is present). The corrected spectra used in fitting can be found in the supplementary material.

As would be expected, the difficulties associated with obtaining a spectrum after triggering the discharge resulted in missing the emission from the plasmoid in some cases. Some of the spectra exhibited only a broad and featureless continuum spanning approximately 2000 cm^{-1}; these spectra were rejected as unusable. Furthermore, there were trials in which we thought that emission from the plasmoid was collected by the instrument, however only instrumental noise was observed in the spectra, which speaks to the importance of triggering the discharge and spectrometer simultaneously.

3.2. Fitting

The PGOPHER [37] program was used to fit the corrected spectra to simulated spectra of water and hydroxyl radical. At the outset of our rotational analysis we attempted to fit a mixture of both

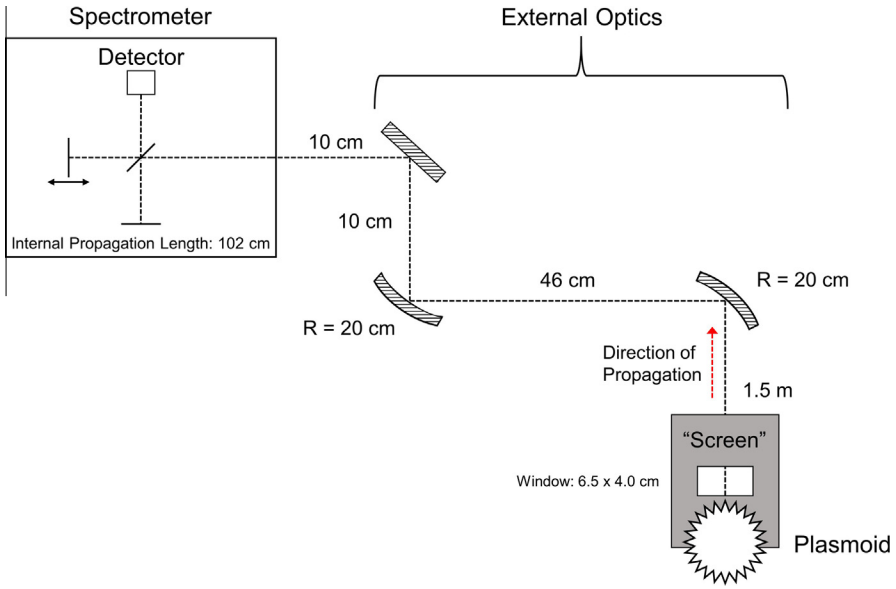

Fig. 3. Bird's eye view of optical setup for experiment. Relevant distances and focal lengths are provided (not to scale).

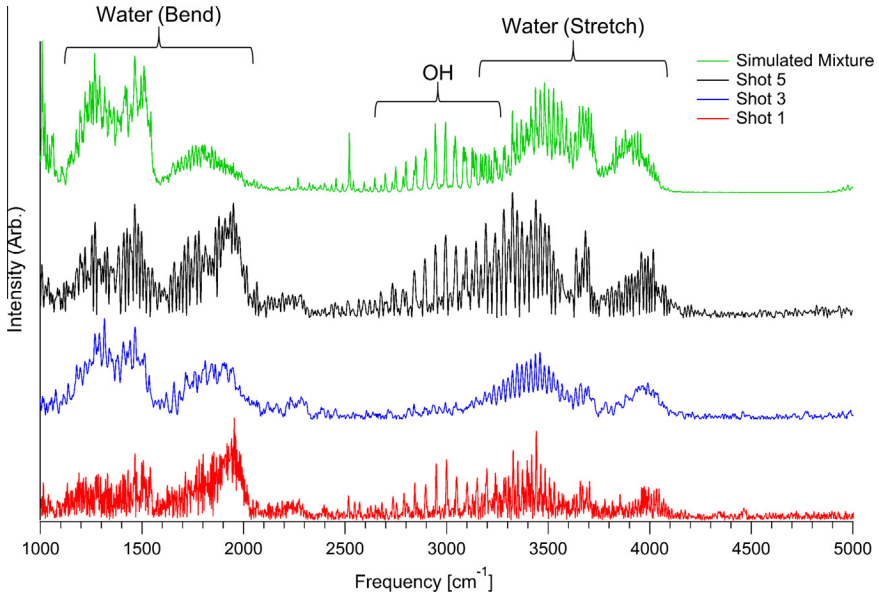

Fig. 4. Upper curve: simulated spectrum of a mixture of H_2O and OH. Lower curves: three examples of emission spectra collected from ball plasmoid discharges, offset for clarity. Spectra were obtained under identical conditions.

of these molecules to the experimental data, however PGOPHER's functionality allows for only a single rotational temperature to be floated during fitting. We expected the temperatures of different plasmoid constituent molecules to be rather different from one another, therefore, each molecule was fit separately. Furthermore, vibrational excitation (and relaxation) occurs differently for each degree of freedom in nonequilibrium air discharges, thus the three vibrational modes of water are also expected to have slightly different values of rotational temperature. The generic fitting procedure involved generating a spectrum of the molecule of interest using the HITRAN line list (imported directly into PGOPHER), modifying the simulation to reflect emission data as per Western's [37] suggestions, overlaying an experimental spectrum in the software, adjusting the scale of the experimental spectra, and finally floating the value for rotational temperature until the fit converged.

When first fitting the data to a spectrum of water we noticed that the fits would converge on a rotational temperature, however some of the residuals appeared to be the result of an unphysical fit. Indeed, when good results were returned from fits to the stretching modes, fits to the bending mode were poor. To resolve this issue, the stretching modes and bending mode of water were analyzed independently; the symmetric and asymmetric stretching modes were fit together, but the bending mode was fit separately. As a result of significant hot band emission, the emission profile of the bending mode was not fully reproduced by the PGOPHER simulations (although hot bands were included in the simulations), resulting in fits taking longer to converge. Fits were performed between 3200–4300 cm^{-1} and 1000–2500 cm^{-1} for the stretching modes and bending mode, respectively (see supplemental material). Numerical results from each of the fits to H_2O are shown in Table 1, and an example of a complete fit is provided in Fig. 5.

Table 1
Calculated rotational temperatures for the vibrational bands of water.

Shot	$T_{rot}^{stretch}$ [K]	T_{rot}^{bend} [K]
1	2300	2000
2	3300	1800
3	1700	2400
4	2200	1400
5	2300	1700
Average	2400 ± 400	1900 ± 300

The rotational temperatures we report show the extent of molecular excitation in the discharge and are comparable to those obtained from the emission of water in oxy-acetylene flames [38].

A similar procedure was used to determine the rotational temperature of hydroxyl radical. The spectra were fit from 2800 to 3200 cm^{-1}, again holding the Lorentzian linewidth constant at 4 cm^{-1}. An example of a fit to OH is shown in Fig. 6, and numerical results of the fits are presented in Table 2. In one particular instance (Shot 3, shown in Fig. 4), the intensity of the signals in the OH emission region were comparable to the noise floor, which resulted in the fits not converging on a rotational temperature. Therefore the values we report for hydroxyl radical are obtained from four separate spectra rather than five. The average rotational temperature of OH was found to be 9200 K, which is high for ambient plasmas. This value is however lower than what has previously been reported for this system [23]; the measurements reported herein were most likely made later in the discharge when compared to those of Versteegh et al. Since the rotational temperature of each constituent molecule must rapidly decrease to room temperature over the course of the discharge, it follows that the rotational temperature would be lower when probing later in the discharge. Time-dependent measurements would be extremely beneficial for the confirmation of rotational temperatures at different stages of the discharge.

There is also an unknown source of emission in the experimental spectra between approximately 2250–2400 cm^{-1}. There are several potential molecular sources for this emission, including CO_2 and CO; the 4.3 μm band of CO_2 [39] and the vibrational band of CO [40] overlap in this region, however this signal is most likely not a result of emission from CO, as the vibrational band of CO is centered approximately 100 wavenumbers to the red of the anomalous feature. We attempted to fit the corrected spectra to a simulation of CO_2 in the same fashion described above, but fits to this molecule did not fully reproduce the shape or intensity of the observed feature, even at high temperatures (see Fig. 7). This region is further complicated by the fact that self-absorption by CO_2 readily occurs in this frequency range. Thus the identity of the cause of the signal in this region remains a mystery; however, the emission profiles shown in Fig. 7 do seem to correspond to that of CO_2 in *some* way. Friday et al. [29] present evidence which suggests that CO_2 may be present in the plasmoid as a result of electrode oxidation, but this does not refute the possibility of gaseous CO_2 emitting from plasmoids produced with a tungsten electrode. Additional measurements of discharges with less shot-to-shot variability would allow for a much more concrete understanding of emission in this region, and improved spectral resolution would allow for a more traditional Boltzmann analysis of a set of known transitions.

The average rotational temperature for OH reported here is limited by the spectral resolution and lack of a thorough Boltzmann analysis, however the procedure used to fit the data provide a reasonable estimate of the rotational temperature. The high temperatures of water and hydroxyl radical indicate that upper vibrational and rotational states of plasmoid constituent molecules are highly populated, which is expected for a nonequilibrium air plasma. These upper states could be populated directly during the discharge via vibrational/rotational excitation processes, or by chemical reactions in the plasmoid. For example, highly-excited OH radicals are thought to be generated by electron impact ionization of water molecules, while other less excited radicals could be generated by excitation of previously-formed OH via other mechanisms. A more thorough analysis of better-resolved transitions could facilitate a two or three temperature model of OH rotational

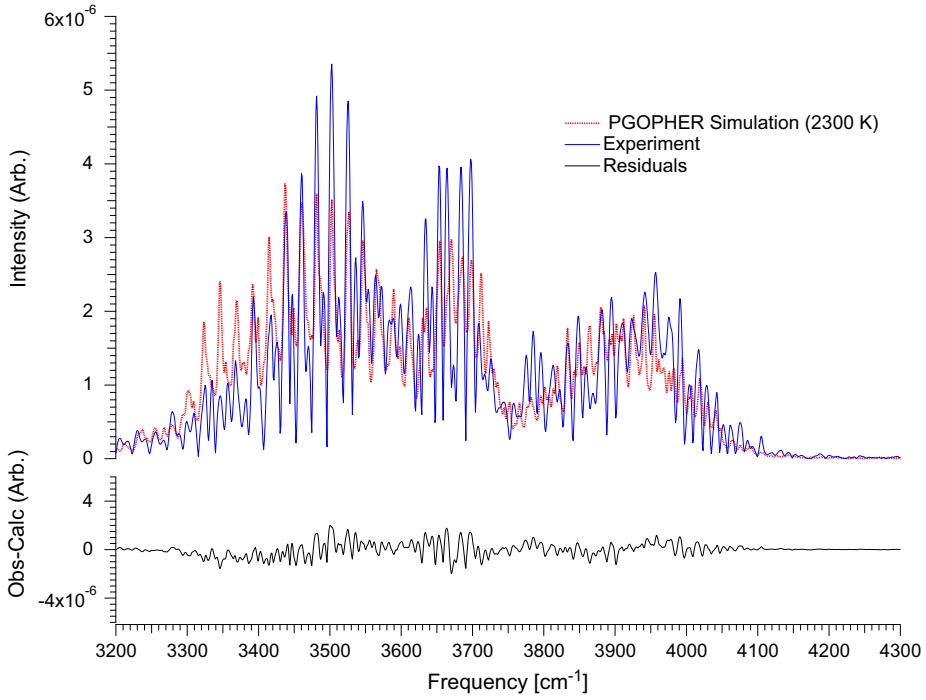

Fig. 5. Example of a fit to the stretching modes of water. This fit is to the spectrum obtained from Shot 4 (see Table 1).

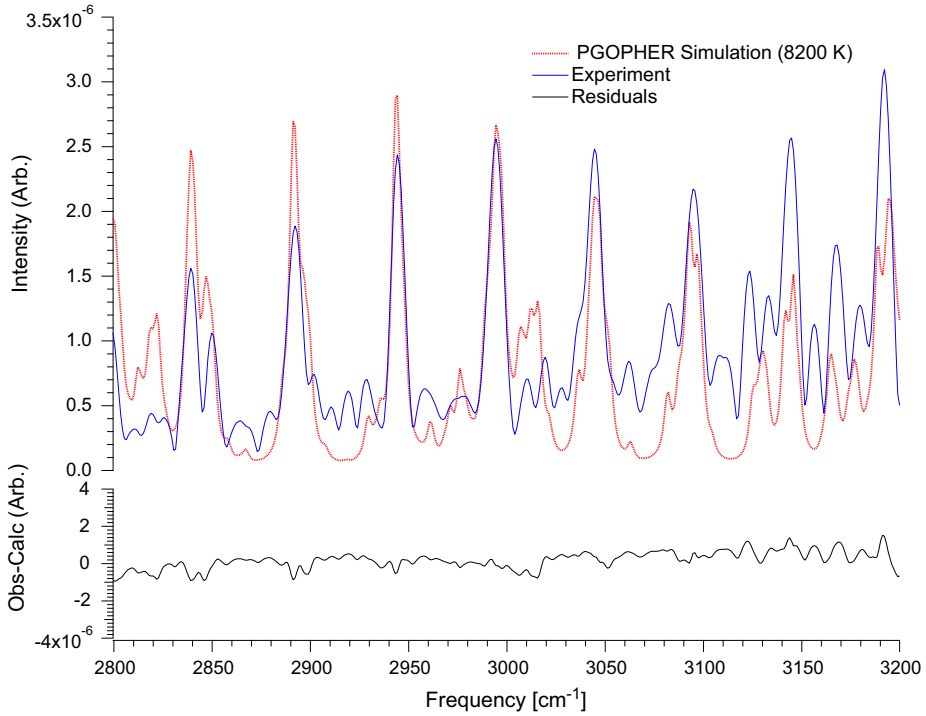

Fig. 6. Example of a fit to hydroxyl radical. This fit is to the spectrum obtained from Shot 2 (see Table 2).

Table 2
Calculated rotational temperatures for hydroxyl radical.

Shot	T_{rot}^{OH} [K]
1	7600
2	8200
3[a]	N/A
4	12,200
5	8600
Average	9200 ± 1500

[a] S/N results in fits that do not converge.

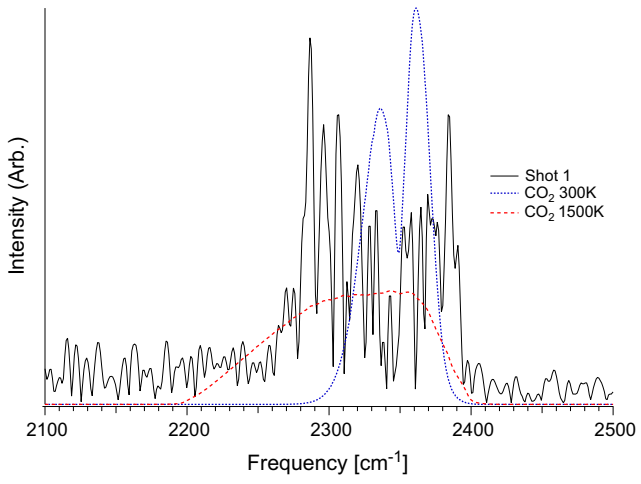

Fig. 7. Comparison of the emission profiles of CO_2 at room and high temperatures to the unexplained signal observed between 2100 and 2400 cm^{-1} in an experimental spectrum (Shot 1 in this case).

distribution, which has been studied extensively in the literature [41,42].

When comparing the spectra collected in this set of experiments to the spectrum presented by Friday et al. [29] (referred to as "the absorption spectrum" here for clarity), several differences can be noted. First, our emission spectra show signals indicative of OH from 2800 to 3200 cm^{-1}, while no evidence of OH absorption is present in the absorption spectrum. Our spectra also show high S/N for all of the vibrational modes of water, while the absorption signals corresponding to the bending mode shown in the absorption spectrum have a much smaller S/N. It is not surprising that the S/N of the bending mode is much greater in the emission spectra – it is likely that the plasmoid is highly vibrationally and rotationally excited and emission from these excited state molecules is occurring frequently. The high temperature of the plasmoid also increases the contribution from vibrational hot band transitions, which are especially prevalent in the bending mode. The two unassigned features presented in the absorption spectrum are not directly observable in our emission spectra, however this does not immediately dismiss the presence of these signals in our spectra as the observed emission profiles are incredibly complex. This complexity is further increased by the possible presence of water clusters in the plasmoid, as many of the rovibrational bands of protonated water clusters are centered within the rovibrational bands of free water molecules [43]. It is unclear at this level of spectral resolution whether emission from protonated water clusters is being detected, but this notion should not be dismissed since the protonated water dimer and trimer have been shown to be present in ball plasmoid discharges [26].

It is difficult to make a direct comparison between emission and absorption spectra collected from ball plasmoid discharges because very little is known about the optical thickness of these plasmoids. Emission spectroscopy of optically thick spheres results in collection of signals from the outermost edge of the sphere, which is not the ideal case for ball plasmoids, as plasmoids have been shown to be surrounded by an "envelope" which is cooler than the interior of the plasmoid [23]. The temperature differences between the interior and exterior of the plasmoid most likely facilitate different chemistry in the center of the plasmoid and at the air–plasmoid interface, and further study of this system with

improved spatial resolution is needed in order to study the different temperature regimes with ball plasmoid discharges.

4. Conclusion

In this work we have presented the first analysis of ball plasmoid emission in the infrared. Using a relatively simple spectroscopic setup, we were able to collect spectra that show emission from water and hydroxyl radical. These molecules are unsurprising to observe in ambient plasma discharges and have been observed in this type of discharge using absorption spectroscopy [29]. We are able to report quantitative information about the plasmoid after reducing the spectral collection time (compared to the three-second acquisition time of Friday et al.), but more importantly this analysis centered on fitting spectra which show rotational structure of constituent molecules. The rotational temperatures that were extracted from the fits of the observed spectra begin to show the energy distribution among molecules in the plasmoid and confirm the measurements of Versteegh et al., reinforcing the fact that ball plasmoid discharges are highly nonthermal and result in rapid heating and rapid cooling of constituent molecules.

In order to move this work forward experimentally and answer the ultimate question of why ball plasmoid recombination occurs much more slowly than is expected, a twofold approach is being undertaken. First, we are expanding the spectral regions in which we are probing; we are working to examine the plasmoid in the near-IR and in the UV/visible to monitor molecules such as N_2^+ and N_2^*. As the principal component of ambient air, it is highly likely that the molecular processes in which nitrogen participates are key to understanding the relaxation processes of the plasmoid. We also plan to re-examine hydroxyl radical with improved spectral and temporal resolution compared to the previous work [23]. This will facilitate a greater understanding of the energy distribution as a function of time and will also provide insight into the reactions which are (or are not) occurring during the three phases of the discharge.

Acknowledgments

We would like to thank Jui-Nung Liu (Cunningham Research Group, UIUC) for his help with operating the spectrometer and for the use of his lab space. S.E.D. would like to thank David M. Friday for starting this project and bringing it with him to UIUC.

Appendix A. Supplementary data

Supplementary data associated with this article can be found, in the online version, at http://dx.doi.org/10.1016/j.jms.2016.02.005. These data include MOL files and InChiKeys of the most important compounds described in this article.

References

[1] Demetre J. Economou, Pulsed plasma etching for semiconductor manufacturing, J. Phys. D – Appl. Phys. 47 (30) (2014).
[2] Hiroaki Kakiuchi, Hiromasa Ohmi, Kiyoshi Yasutake, Atmospheric-pressure low-temperature plasma processes for thin film deposition, J. Vac. Sci. Technol. A 32 (3) (2014).
[3] Mohammed Yousfi, Nofel Merbahi, Atul Pathak, Olivier Eichwald, Low-temperature plasmas at atmospheric pressure: toward new pharmaceutical treatments in medicine, Fundam. Clin. Pharmacol. 28 (2) (2014) 123–135.
[4] Gregory Fridman, Gary Friedman, Alexander Gutsol, Anatoly B. Shekhter, Victor N. Vasilets, Alexander Fridman, Applied plasma medicine, Plasma Process. Polym. 5 (6) (2008) 503–533.
[5] David B. Graves, Low temperature plasma biomedicine: a tutorial review, Phys. Plasmas 21 (8) (2014).
[6] G.B. McCombs, M.L. Darby, New discoveries and directions for medical, dental and dental hygiene research: low temperature atmospheric pressure plasma, Int. J. Dent. Hyg. 8 (1) (2010) 10–15.
[7] Gang Xiao, Weiping Xu, Rongbing Wu, Mingjiang Ni, Changming Du, Xiang Gao, Zhongyang Luo, Kefa Cen, Non-thermal plasmas for VOCs abatement, Plasma Chem. Plasma Process. 34 (5) (2014) 1033–1065.
[8] E. Tatarova, N. Bundaleska, J. Ph Sarrette, C.M. Ferreira, Plasmas for environmental issues: from hydrogen production to 2D materials assembly, Plasma Sources Sci. Technol. 23 (6) (2014).
[9] Ravindra B. Sabnis, Amit Bhattu, Vijaykumar Mohankumar, Sterilization of endoscopic instruments, Curr. Opin. Urol. 24 (2) (2014) 195–202.
[10] M. Moreau, N. Orange, M.G.J. Feuilloley, Non-thermal plasma technologies: new tools for bio-decontamination, Biotechnol. Adv. 26 (6) (2008) 610–617.
[11] M. Moisan, J. Barbeau, S. Moreau, J. Pelletier, M. Tabrizian, L.H. Yahia, Low-temperature sterilization using gas plasmas: a review of the experiments and an analysis of the inactivation mechanisms, Int. J. Pharmaceut. 226 (1–2) (2001) 1–21.
[12] Anne Mai-Prochnow, Anthony B. Murphy, Keith M. McLean, Michael G. Kong, Kostya (Ken) Ostrikov, Atmospheric pressure plasmas: infection control and bacterial responses, Int. J. Antimicrob. Agents 43 (6) (2014) 508–517.
[13] J. Ehlbeck, U. Schnabel, M. Polak, J. Winter, Th. von Woedtke, R. Brandenburg, T. von dem Hagen, K.-D. Weltmann, Low temperature atmospheric pressure plasma sources for microbial decontamination, J. Phys. D – Appl. Phys. 44 (1) (2011).
[14] Xue Zhang, Xiao-Fei Zhang, He-Ping Li, Li-Yan Wang, Chong Zhang, Xin-Hui Xing, Cheng-Yu Bao, Atmospheric and room temperature plasma (ARTP) as a new powerful mutagenesis tool, Appl. Microbiol. Biotechnol. 98 (12) (2014) 5387–5396.
[15] Rohit Thirumdas, Chaitanya Sarangapani, Uday S. Annapure, Cold plasma: a novel non-thermal technology for food processing, Food Biophys. 10 (1) (2015) 1–11.
[16] N.N. Misra, B.K. Tiwari, K.S.M.S. Raghavarao, P.J. Cullen, Nonthermal plasma inactivation of food-borne pathogens, Food Eng. Rev. 3 (3-4) (2011) 159–170.
[17] C. Meyer, S. Mueller, E.L. Gurevich, J. Franzke, Dielectric barrier discharges in analytical chemistry, Analyst 136 (12) (2011) 2427–2440.
[18] Jacob T. Shelley, Joshua S. Wiley, George C.Y. Chan, Gregory D. Schilling, Steven J. Ray, Gary M. Hieftje, Characterization of direct-current atmospheric-pressure discharges useful for ambient desorption/ionization mass spectrometry, J. Am. Soc. Mass Spectrom. 20 (5) (2009) 837–844.
[19] Anastasia Albert, Jacob T. Shelley, Carsten Engelhard, Plasma-based ambient desorption/ionization mass spectrometry: state-of-the-art in qualitative and quantitative analysis, Anal. Bioanal. Chem. 406 (25) (2014) 6111–6127.
[20] A.I. Egorov, S.I. Stepanov, Long-lived plasmoids produced in humid air as analogues of ball lightning, Tech. Phys. 47 (12) (2002) 1584–1586.
[21] Claire Tendero, Christelle Tixier, Pascal Tristant, Jean Desmaison, Philippe Leprince, Atmospheric pressure plasmas: a review, Spectrochim. Acta Part B: Atom. Spectrosc. 61 (1) (2006) 2–30.
[22] Noriyuki Hayashi, Hiroko Satomi, Toshinori Kajiwara, Tetsuo Tanabe, Properties of ball lightning generated by a pulsed discharge on surface of an electrolyte in the atmosphere, IEEJ Trans. Electr. Electron. Eng. 3 (6) (2008) 731–733.
[23] A. Versteegh, K. Behringer, U. Fantz, G. Fussmann, B. Jüttner, S. Noack, Long-living plasmoids from an atmospheric water discharge, Plasma Sources Sci. Technol. 17 (2) (2008) 024014.
[24] Youichi Sakawa, Kazuyoshi Sugiyama, Tetsuo Tanabe, Richard More, Fireball generation in a water discharge, Plasma Fusion Res. 1 (2006) (039-039).
[25] Karl D. Stephan, Shelby Dumas, Laurence Komala-Noor, Jonathan McMinn, Initiation, growth and plasma characteristics of "gatchina water plasmoids, Plasma Sources Sci. Technol. 22 (2) (2013) 025018.
[26] Scott E. Dubowsky, David M. Friday, Kevin C. Peters, Zhangji Zhao, Richard H. Perry, Benjamin J. McCall, Mass spectrometry of atmospheric-pressure ball plasmoids, Int. J. Mass Spectrom. 376 (0) (2015) 39–45.
[27] Pang Xuexia, Deng Zechao, Jia Pengying, Liang Weihua, Li Xia, Influence of ionization degrees on the evolutions of charged particles in atmospheric plasma at low altitude, Plasma Sci. Technol. 14 (8) (2012) 716.
[28] Yukinori Sakiyama, David B. Graves, Hung-Wen Chang, Tetsuji Shimizu, Gregor E. Morfill, Plasma chemistry model of surface microdischarge in humid air and dynamics of reactive neutral species, J. Phys. D: Appl. Phys. 45 (42) (2012) 425201.
[29] David M. Friday, Peter B. Broughton, Tanner A. Lee, Garrett A. Schutz, Jeremiah N. Betz, C. Michael Lindsay, Further insight into the nature of ball-lightning-like atmospheric pressure plasmoids, J. Phys. Chem. A 117 (39) (2013) 9931–9940.
[30] Jianyong Cen, Ping Yuan, Simin Xue, Observation of the optical and spectral characteristics of ball lightning, Phys. Rev. Lett. 112 (2014) 035001.
[31] John Abrahamson, Ball lightning from atmospheric discharges via metal nanosphere oxidation: from soils, wood or metals, Philos. Trans. Royal Soc. Lond. Ser. A: Math., Phys. Eng. Sci. 360 (1790) (2002) 61–88.
[32] Karl D. Stephan, Electrostatic charge bounds for ball lightning models, Phys. Scripta 77 (3) (2008) 035504.
[33] A.V. Shavlov, The two-temperature plasma model of a fireball. The calculated parameters, Phys. Lett. A 373 (43) (2009) 3959–3964.
[34] K. Tennakone, Stable spherically symmetric static charge separated configurations in the atmosphere: implications on ball lightning and earthquake lights, J. Electrostat. 69 (6) (2011) 638–640.

[35] S.V. Shevkunov, Cluster mechanism of the energy accumulation in a ball electric discharge, Doklady Phys. 46 (7) (2001) 467–472.
[36] L.S. Rothman, D. Jacquemart, A. Barbe, D. Chris Benner, M. Birk, L.R. Brown, M. R. Carleer, C. Chackerian Jr., K. Chance, L.H. Coudert, V. Dana, V.M. Devi, J.-M. Flaud, R.R. Gamache, A. Goldman, J.-M. Hartmann, K.W. Jucks, A.G. Maki, J.-Y. Mandin, S.T. Massie, J. Orphal, A. Perrin, C.P. Rinsland, M.A.H. Smith, J. Tennyson, R.N. Tolchenov, R.A. Toth, J. Van der Auwera, P. Varanasi, G. Wagner, The HITRAN 2004 molecular spectroscopic database, J. Quant. Spectrosc. Radiat. Transf. 96 (2) (2005) 139–204.
[37] C.M. Western, PGOPHER, A Program for Simulating Rotational Structure, University of Bristol. <http://pgopher.chm.bris.ac.uk>.
[38] Pierre-Franois Coheur, Peter F. Bernath, Michel Carleer, Reginald Colin, Oleg L. Polyansky, Nikolai F. Zobov, Sergei V. Shirin, Robert J. Barber, Jonathan Tennyson, A 3000k laboratory emission spectrum of water, J. Chem. Phys. 122 (7) (2005).
[39] C.C. Ferriso, C.B. Ludwig, L. Acton, Spectral-emissivity measurements of the 4.3-μ CO_2 band between 2650° and 3000°, J. Opt. Soc. Am. 56 (2) (1966) 171–173.
[40] K.P. Huber, G. Herzberg, Molecular Spectra and Molecular Structure: IV. Constants of Diatomic Molecules, Springer, US, 1979.
[41] H. Meinel, L. Krauss, ber die besetzung der rotationszustnde von oh und c2 in niederdruckplasmen, J. Quant. Spectrosc. Radiat. Transf. 9 (3) (1969) 443–460.
[42] C.I.M. Beenakker, F.J. De Heer, H.B. Krop, G.R. Mhlmann, Dissociative excitation of water by electron impact, Chem. Phys. 6 (3) (1974) 445–454.
[43] Jeffrey M. Headrick, Eric G. Diken, Richard S. Walters, Nathan I. Hammer, Richard A. Christie, Jun Cui, Evgeniy M. Myshakin, Michael A. Duncan, Mark A. Johnson, Kenneth D. Jordan, Spectral signatures of hydrated proton vibrations in water clusters, Science 308 (5729) (2005) 1765–1769.